Defence Research and Development Canada
Recherche et développement pour la défense Canada

DEFENCE R&D DÉFENSE

Micro-Doppler radar signatures for intelligent target recognition

T. Thayaparan, S. Abrol and E. Riseborough

Defence R&D Canada – Ottawa
TECHNICAL MEMORANDUM
DRDC Ottawa TM 2004-170
September 2004

Canada

Micro-Doppler radar signatures for intelligent target recognition

T. Thayaparan
Defence R&D Canada – Ottawa

S. Abrol
University of Ottawa

E. Riseborough
Defence R&D Canada – Ottawa

Defence R&D Canada – Ottawa

Technical Memorandum

DRDC Ottawa TM 2004-170

September 2004

Abstract

Mechanical vibrations or rotations (micro-motion dynamics) of structures on a target may introduce frequency modulation on the radar return from the target's body. The modulation due to this vibration or rotation is referred to as the micro-Doppler (m-D) phenomenon. In this report, the m-D effect is introduced and the mathematics of micro-Doppler signatures, induced by simple sinusoidal vibrations or rotations, is developed. Simulated results confirm that the mathematical analysis is valid. The m-D features derived from a target's vibrational/rotational motion are extracted by utilizing discrete wavelet transforms. During this process, the time domain radar signal is decomposed into a set of components that are represented by different wavelet scales. The m-D features are extracted by sorting the components that are associated with the vibrational/rotational motions of a target and is achieved by applying the inverse wavelet transform. After the extraction of m-D features, time-frequency analysis is employed to analyze the oscillation and to estimate the motion parameters. The vibration/rotation rate is estimated by taking the autocorrelation of the time sequence data. The findings show that these results have higher precision after the m-D extraction since only vibrational/rotational components are employed. The proposed method of the m-D extraction has been successfully applied to both simulated data and experimental helicopter and human data. The preliminary results clearly demonstrate that the m-D signatures can be observed by radar and suggest that applications of m-D should be investigated and exploited for target detection, classification and recognition. It is recommended that the exploitation of micro-Doppler, as a new identification/recognition tool, be undertaken as it could impact all aspects of radar sensing and may enhance the effectiveness of Automatic Target Recognition (ATR) and Automatic Gait Recognition (AGR) techniques. We recommend that a new man-portable "micro-Doppler radar" be constructed for use on the battlefield or for disaster scenarios. We also propose a sequence of research work to achieve the desired technical objectives.

Résumé

Les rotations ou vibrations mécaniques (dynamique de micro-mouvement) des structures d'une cible peuvent engendrer la modulation de fréquence des échos radar provenant du corps de la cible. La modulation due à ces rotations ou vibrations est appelée effet micro-Doppler (m-D). Ce rapport présente l'effet m-D et aborde les aspects mathématiques des signatures micro-Doppler, dues à des rotations ou à des vibrations sinusoïdales simples. Les résultats simulés confirment que l'analyse mathématique est valide. Les caractéristiques m-D causées par les rotations/vibrations d'une cible sont extraites au moyen de transformées à ondelettes discrètes. Durant ce procédé, le signal radar dans le domaine temporel est décomposé en un ensemble de composantes représentées par des échelles d'ondelettes différentes. Les caractéristiques m-D sont extraites par le tri des composantes associées aux mouvements de rotation/vibration d'une cible et elles sont établies par l'application de la transformée d'ondelette inverse. Après l'extraction des caractéristiques m-D, on recourt à une analyse temps-fréquence pour analyser l'oscillation et pour estimer les paramètres de mouvement. Le taux de rotation/vibration est estimé par l'autocorrélation des données de la séquence temporelle. Cette procédure démontre que les résultats présentent une précision accrue après l'extraction m-D, car seules les composantes de rotation/vibration sont employées. La méthode proposée d'extraction m-D a été appliquée avec succès à des données simulées ainsi qu'à des données expérimentales provenant d'hélicoptères et d'humains. Les résultats préliminaires démontrent clairement que les signatures m-D peuvent être observées dans les échos radar et donnent à penser que des applications m-D devraient être étudiées et exploitées pour la détection, la classification et la reconnaissance des cibles. Il est recommandé d'entreprendre l'exploitation de l'effet micro-Doppler comme nouvel outil d'identification et de reconnaissance, car cet outil pourrait avoir une incidence sur tous les aspects de la détection radar et améliorer l'efficacité des techniques de reconnaissance automatique des cibles (ATR) et de reconnaissance automatique de la démarche (AGR). Nous recommandons la fabrication d'un nouveau radar micro-Doppler portable pouvant s'utiliser sur le champ de bataille ou en cas de catastrophe. Nous proposons aussi une séquence de travaux de recherche permettant d'atteindre les objectifs techniques désirés.

Executive summary

Mechanical vibrations or rotations of a target or structures on the target may induce additional frequency modulations on the returned radar signal which generate sidebands about the target's body return Doppler frequency. These frequency modulations are called the micro-Doppler (m-D) effect. The m-D signatures enable certain properties of the target to be determined that may be used for target recognition. In this report, the m-D effect in radar is introduced and the mathematics of m-D signatures induced by simple sinusoidal vibrations or rotations is developed. Computer simulations are conducted and m-D features in the time-scale and time-frequency domains are expoited. Both the simulation and experimental helicopter and human results confirm that the mathematical analysis is valid. The results clearly demonstrate that the m-D effect can be observed in radar returns and suggest that applications of m-D should be further investigated and exploited.

As a identification/recognition tool, m-D is a promising candidate for operational target recognition systems that could enhance the effectiveness of the radar target recognition. The m-D radar signature can distinguish important classes of battlefield targets. The m-D signatures of vibrating and rotating structures can be used to differentiate and identify specific types of military vehicles/tanks. This approach could provide improved target signature/feature recognition over current audio classification and jet engine modulation techniques [30-33]. In addition to battlefield land targets, important classes of air targets can also be distinguished by their m-D signatures. For example, radar signals returned from military targets that incorporate vibrating or rotating structures such as aircraft propellers, helicopter rotors, jet engine compressor and blade assemblies, rotating antennas on a ship or an aircraft contain m-D signatures related to these structures. Hence the m-D effects offer a new way for the analysis of military target signatures and help our military and security agencies to better detect and identify potential threats using all-weather surveillance radars. It provides additional and unique target features that are complementary to those made available by existing methods.

Radar gait image analysis integrated with m-D can provide new identification methods for remote detection of walking personnel either in battlefield or urban scenarios. This technique can be applied to other areas as well: countering terrorism, conducting urban military operations, providing urban border security, dealing with hostage acts, intercepting suicide bombers, and detecting humans (soldiers) in a forest. This new identification method could also provide a surveillance technology for identifying humans at a distance by their walk. Distance is the key, because terrorists and other criminals often act from afar, and the earliest detection means a quicker response. Therefore, as a new identification/recognition tool for an operational radar Automatic Gait Recognition (AGR) system, m-D has good potential for significantly improving military capabilities and protection for CF and CF facilities.

It is recommended that the exploitation of micro-Doppler, as a new identification/recognition tool, be undertaken as it could impact all aspects of radar

sensing and may enhance the effectiveness of Automatic Target Recognition (ATR) and Automatic Gait Recognition (AGR) techniques. We recommend that a new man-portable "micro-Doppler radar" be constructed for use on the battlefield or disaster scenarios. We also propose a sequence of research work to achieve the desired technical objectives.

T. Thayaparan , S. Abrol , E. Riseborough . 2004. Micro-Doppler radar signatures for intelligent target recognition. DRDC Ottawa TM 2004-170. Defence R&D Canada – Ottawa.

Sommaire

Les rotations ou vibrations mécaniques d'une cible ou des structures d'une cible peuvent engendrer la modulation de fréquence supplémentaire des échos radar, ce qui produit des bandes latérales de part et d'autre de la fréquence Doppler provenant du corps de la cible. Cette modulation de fréquence est appelée effet micro-Doppler (m-D). Les signatures m-D permettent de déterminer certaines propriétés pouvant servir à la reconnaissance des cibles. Ce rapport présente l'effet m-D et aborde les aspects mathématiques des signatures m-D, dues à des rotations ou à des vibrations sinusoïdales simples. Des simulations par ordinateur sont exécutées et les caractéristiques m-D sur l'échelle temporelle et dans les domaines temps-fréquence sont exploitées. La simulation et les résultats expérimentaux provenant d'hélicoptères et d'humains confirment que l'analyse mathématique est valide. Les résultats démontrent clairement que l'effet m-D peut être observé dans les échos radar et donnent à penser que les applications m-D devraient être étudiées plus en profondeur et exploitées.

En tant qu'outil d'identification et de reconnaissance, l'effet m-D semble prometteur pour les systèmes opérationnels susceptibles d'améliorer l'efficacité de la reconnaissance des cibles radar. La signature radar m-D permet de distinguer les classes importantes de cibles sur le champ de bataille. Les signatures m-D des structures tournantes et vibrantes peuvent servir à différencier et à identifier des types particuliers de véhicules militaires/chars. Cette façon de procéder pourrait améliorer la reconnaissance des signatures/caractéristiques des cibles par rapport aux techniques actuelles fondées sur la classification audio et la modulation des réacteurs [30-33]. Outre les cibles terrestres des champs de bataille, des classes importantes de cibles aériennes peuvent aussi se distinguer d'après leur signature m-D. Par exemple, les signaux radar provenant de cibles militaires dotées de structures tournantes ou vibrantes, comme les hélices d'aéronef, les rotors d'hélicoptère, les ensembles à compresseur de réacteur et pales et les antennes tournantes d'un navire ou d'un aéronef, portent la signature m-D de ces structures. Les effets m-D offrent donc une nouvelle façon d'analyser les signatures des cibles militaires et aident nos organismes militaires et de sécurité à mieux détecter et identifier les menaces possibles au moyen de radars de surveillance tous temps. Cette technique d'analyse révèle des caractéristiques de cibles additionnelles et uniques, complémentaires par rapport à celles que fournissent les méthodes existantes.

L'analyse radar de la démarche, intégrée à la technique m-D, peut fournir de nouvelles méthodes d'identification pour la télédétection du personnel en marche sur les champs de bataille ou dans des zones urbaines. Cette technique peut aussi s'appliquer à d'autres secteurs, notamment la lutte contre le terrorisme, les opérations militaires urbaines, la sécurité frontalière urbaine, les prises d'otages, l'interception des éventuels auteurs d'attentats suicides et la détection des humains (soldats) dans une forêt. De plus, elle pourrait fournir les moyens de surveillance nécessaires pour identifier des humains éloignés, d'après leur démarche. Cet éloignement est crucial, car les terroristes et les autres criminels agissent souvent à une certaine distance, et une détection rapide se

traduit par une réaction rapide. Employée comme nouvel outil d'identification et de reconnaissance dans un système de reconnaissance automatique de la démarche (AGR) à radar opérationnel, la technique m-D pourrait fort bien améliorer de façon notable les capacités militaires et la protection des FC et de leurs installations.

Il est recommandé d'entreprendre l'exploitation de l'effet micro-Doppler comme nouvel outil d'identification et de reconnaissance, car cet outil pourrait avoir une incidence sur tous les aspects de la détection radar et améliorer l'efficacité des techniques de reconnaissance automatique des cibles (ATR) et de reconnaissance automatique de la démarche (AGR). Nous recommandons la fabrication d'un nouveau radar micro-Doppler portable pouvant s'utiliser sur le champ de bataille ou en cas de catastrophe. Nous proposons aussi une séquence de travaux de recherche permettant d'atteindre les objectifs techniques désirés.

T. Thayaparan , S. Abrol , E. Riseborough . 2004. Micro-Doppler radar signatures for intelligent target recognition. DRDC Ottawa TM 2004-170. R & D pour la défense Canada – Ottawa.

Table of contents

List of figures

1. Introduction

Target recognition is an essential operation in military radar applications. Rapid and reliable identification of targets at maximum surveillance and weapon system range remains a challenging problem. The inability to identify hostile targets in land, air, and maritime missions is considered one of the most serious deficiencies in Canadian Forces (CF) and NATO's defence capability [1-2]. Real-time Automatic Target Recognition (ATR) techniques are identified as potential solutions for attaining accurate hostile target identification. Real-Time Automatic Gait Recognition (AGR) radar systems have recently been recognized as potential solutions for detecting, classifying and identifying human targets at distance in all weather conditions [3-5]. Such capabilities could enhance the protection of CF and facilities from terrorist attacks. From the CF operational perspective, the development of new ATR and AGR methods could enhance self-defence capabilities of the CF in land, air, and maritime through advanced methods for threat assessment, threat detection, identification and kill assessment. These are areas of high challenge and promising potential that require thorough investigation. This report along with the proposed future studies will lead to unique ATR and AGR capabilities for accurately estimating the tactical picture and for a rapid response to asymmetrical threats.

When the radar transmits an electromagnetic signal to a target, the signal interacts with the target and then returns to the radar. The change in the properties of the returned signal reflects on the characteristics of the target. When the target is moving, the carrier frequency of the returned signal will be shifted due to Doppler effect. The Doppler frequency shift can be used to determine the radial velocity of the moving target. If the target or any structure on the target is vibrating or rotating in addition to target translation, it will induce frequency modulation on the returned signal that generates sidebands about the target's Doppler frequency. This modulation is called the micro-Doppler (m-D) phenomenon. The m-D phenomenon can be regarded as a characteristic of the interaction between the vibrating or rotating structures and the target body. If the target undergoes a vibration or rotation, then the Doppler frequency shift generated by the vibration or rotation is a time-varying function and imposes a periodic time-varying modulation onto the carrier frequency. The modulation contains harmonic frequencies that depend on the carrier frequency, the vibration or rotation rate, and the angle between the direction of vibration and the direction of the incident wave. While the Doppler frequency induced by the target body is constant, the m-D due vibrating or rotating structure of the target is a function of dwell time. The micro-Doppler effect was originally introduced in laser systems, but it can also be observed in microwave radar systems. The fundamental research of the m-D phenomenon in radar is a relatively unexplored and untested area [5].

Micro-Doppler radar signatures of battlefield engine are caused by vibration. In many cases, a target or any structure on the target may have vibrations or rotations that are referred to micro-motion dynamics. For example, vibrations generated by a vehicle engine may be detected from the surface vibration of the vehicle. From the m-D

signature of engine vibration signals, one can further distinguish a gas turbine engine of a tank from a diesel engine of a bus. Vehicles produce their own types of m-D signature as do helicopters. Therefore, the m-D effect can be used to identify specific types of battlefield targets and determine their movement and engine speed. This approach can provide improved target recognition/feature recognition over current audio classification techniques [30-33]. In addition to battlefield land targets, important classes of air targets, such as helicopters and aircrafts that may have vibrations or rotations in addition to target translation, can also be distinguished by their m-D signatures. These signatures consist of the jet engine modulation lines caused by the rotating blades of the jet engine turbines and, for helicopter in particular, the m-D signature components created by many moving parts of the main and tail rotor assemblies. Hence, m-D offers a new approach for target signature analysis by isolating additional and unique target features that are complementary to those used by existing methods. One of the problems with aircraft identification using jet engine modulation signatures is the complexity of the signal [33]. Because of this complexity its exact nature is difficult to define. This requires more refined signal processing techniques in order to extract the relevant information from background noise, clutter and extraneous harmonics. Traditional spectral analysis techniques have been developed, however, the signal-processing task is often complicated by a low signal-to-noise ratio (SNR) and the presence of spurious spectral lines introduced by the radar. Research on the methodology for extracting m-D features has to be carried out to demonstrate the full impact of this innovative approach on future intelligent automatic target recognition. Traditional analyses, such as Fourier analysis or the sliding window FFT (short time Fourier transform), lack the necessary resolution for extracting and processing these unique features. Therefore, high-resolution analysis is necessary for analyzing m-D information. Promising alternatives for these cases are techniques that are based on time-frequency or time-scale signal processing methods [6-25]. The preliminary simulated and experimental results presented in this report indicate that this approach is feasible and can yield the desired results.

Obtaining radar signatures of personnel is another important application of m-D. The human walking gait is a complex motion behaviour that comprises different movements of individual body parts. Since September 11, Automatic Gait Recognition (AGR) technology is growing in significance. Because gait recognition technology is so new, researchers are assessing its uniqueness and methods by which it can be evaluated. Various computer vision and ultrasound techniques have been developed to measure gait parameters [26-29]. Real-Time AGR radar systems have recently been recognized as advantageous solutions for detecting, classifying and identifying human targets at distances in all light and weather conditions. Radar has certain advantages over electro optical (EO) systems and video cameras in that it can penetrate into clothes, does not require light, and operates in fog and other low-visibility weather conditions. However, radar-based recognition is such a novel approach that much fundamental research has yet to be done in this area. The radar sends out a signal and then measures the echo that contains rich information about the various parts of the moving body. There are different shifts for different body parts, because they are moving at different velocities.

For example, a walking man with swinging arms may induce frequency modulation of the returned signal and generate sidebands about the body Doppler. In this report, we develop the preliminary ground work for this challenging field of research.

The report is organized as follows. Section 2 provides a introduction to the mathematical description of the m-D phenomenon. Section 3 briefly discusses the wavelet theory relevant to this application and gives a detailed treatment of m-D feature extraction using wavelet digital filter banks. Section 4 briefly describes the radar system parameters used in the simulated and experimental data. Results are presented in Section 5 that show that m-D features can be accurately extracted using wavelet transform method. The motion parameters are estimated with the time-frequency analysis and auto-correlation techniques. The sensitivity of the proposed method is also discussed. Conclusions and recommendations for future studies are given in section 6.

2. Mathematical description of the micro-Doppler phenomenon

The mathematical description of m-D phenomenon induced by vibrational motions is discussed in this section. The rotation could be seen as a special case of vibration. In coherent radar, the variations in range cause phase change on a returned signal from a target. A half-wavelength change in range can cause 360-degree phase change. It is conceivable that the vibration of a reflecting surface may be measured with the phase change. Thus, the Doppler frequency shift that represents the change of phase function with time, can be used detect vibrations or rotations of structures in a target [5]. Mathematics of the m-D effect can be derived by introducing vibration or rotation (micro-motion) to the conventional Doppler analysis. A target can be represented as a set of point scatterers, which are the primary reflecting points on the target. The point scattering model can simplify the analysis while preserving the m-D induced by micro-motions. In our case, there exists a vibrating point scatterer in a radar-returned signal. The received Doppler from a target as a function of time, is modeled by the following equation

(1) $$s(t) = A\exp[j(2\pi f_0 t + \phi(t))]$$

where A is the reflectivity of the vibrating point scatterer, f_0 is the carrier frequency of the transmitted signal. The $\phi(t)$ is the time-varying phase change of the vibrating scatterer. Assuming that the vibrating scatterer is set to a radian frequency oscillation of ω_ν , the time-varying phase is

(2) $$\phi(t) = \beta\sin(\omega_\nu)$$

where $\beta = 4\pi D_\nu/\lambda$, D_ν is amplitude of the vibration and λ is the wavelength of the transmitted signal [3]. Substituting equation (2) into equation (1) yields

(3) $$s(t) = A\exp[j(2\pi f_0 t + \beta\sin(\omega_\nu t))]$$

The equation (3) may be written in a Fourier series expansion as follows

(4) $$s(t) = A\sum_{n=-\infty}^{\infty} c_n e^{j(2\pi f_0 + n\omega_\nu)t}$$

The Fourier coefficient c_n will be expressed as

(5) $$c_n = \frac{1}{2\pi}\int_{-\pi}^{\pi} e^{j\beta\sin\omega_\nu t} e^{-jn\omega_\nu t} dt = J_n(\beta)$$

which is an nth-order Bessel function of first kind [5]. Substituting equation (5) into (3) yields

(6) $$s(t) = A\sum_{n=-\infty}^{\infty} J_n(\beta)\exp[j(2\pi f_0 + n\omega_\nu)t]$$

The equation (6) shows a m-D frequency spectrum that consists of pairs of harmonic spectral lines around the center frequency f_0. The spacing between adjacent spectral lines is $\omega_\nu/2\pi$. Furthermore, since the phase term function in equation (3) is time varying, the instantaneous frequency f_D, i.e., the m-D frequency induced by the vibration of scatterer, may be expressed as

(7) $$f_D = \frac{1}{2\pi}\frac{d\phi}{dt} = \frac{1}{2\pi}\beta\omega_\nu\cos(\omega_\nu t) = \frac{2}{\lambda}D_\nu\omega_\nu\cos(\omega_\nu t)$$

Note that the maximum m-D frequency change is $(2/\lambda)D_\nu\omega_\nu$, which is used to estimate the displacement of a vibrating scatterer. The m-D induced by vibration is a sinusoidal function of time at the vibrating frequency ω_ν. Usually, when the vibrating modulation is small, it is difficult to detect the vibration in the frequency domain. Thus, a method that is able to separate the radar return induced by the target body from that induced by its vibrating structure might help to isolate the vibrating spectrum from other contributions.

This new technology can be developed for m-D applications of military significance (e.g., helicopters rotors; aircraft propellers; the jet engine modulation of an air target, rotating ship or aircraft antennas; the human walking gait analysis; vibrations of a vehicle/tank; etc.).

Modulation induced by rotation structures can be regarded as a unique signature of a target. This m-D signature is an important feature for identifying targets of interest (i.e. helicopters, ships or aircraft with rotating antennas). When there is a rotating scatterer on a target, the phase term in equation (2) may be expanded as follows

(8) $$\phi(t) = \beta\sin(\Omega t + \theta_0)$$

where Ω is the rotation rate and θ_0 is the rotating angle of the scatterer on the rotating structure at $t = 0$, called initial rotating angle. Therefore, the received Doppler from one rotating scatterer may be expressed by the equation (9), which is an expansion of a vibrating structure, i.e.

(9) $$s(t) = A\exp[j(2\pi f_0 t + \beta\sin(\Omega t + \theta_0))]$$

Equation (9) may also be expressed by the Bessel function of the first kind. Similar to Equation (6), m-D consists of harmonic spectral lines around center frequency. If there are N rotating scatterers on a target (such as the rotor blades of a helicopter), there will be N different initial rotating angles, i.e.

(10) $$\theta_k = \theta_0 + k2\pi/N$$

for $k = 0, ..., N-1$; and thus the total received signal becomes

(11) $$s(t) = \sum_{k=0}^{N-1} A\exp[j(2\pi f_0 t + \beta\sin(\Omega t + \theta_0 + k2\pi/N))]$$

3. Wavelet expansion of signal

The structure that induces m-D features change at a rate much faster than the target itself. Wavelet analysis has the capability of detecting rapid changes of the signal [21-25]. Therefore, the wavelet transform can be considered as a powerful tool for extracting m-D features. Wavelet transforms of the data can be achieved by using a tree of digital filter banks based upon the multi-resolution analysis theory [24]. In this section, the theory of wavelets relevant to the extraction of m-D features is presented. A more comprehensive discussion on wavelets may be found in references [22-25].

3.1 Basic concept and definition

Multi-resolution analysis is performed by orthonormal wavelet transforms based on a scaling function. A function called the "mother wavelet" includes dilations (scales) and translations (time-shifted) as follows

$$\psi_{m,n} = 2^{m/2}\psi(2^m t - n) \tag{12}$$

and forms an orthogonal basis of $L^2(R)$. The wavelet basis generates an orthogonal decomposition of $L^2(R)$, i.e.

$$L^2(R) = \oplus_m W_m \tag{13}$$

where W_m is a subspace spanned by $\{\psi_{m,n}(t)\}_{n=-\infty}^{n=\infty}$, while the symbol $\oplus$ denotes "direct sum" and means that these subspace meet only in zero function [24].

The wavelet basis is generated from a scaling function $\varphi(t)$ basis through the following "dilation" equations. These two bases are mutually orthogonal at each resolution level:

$$\varphi(t) = \sqrt{2}\sum_k L_k \varphi(2t - k) \tag{14}$$

$$\psi(t) = \sqrt{2}\sum_k H_k \varphi(2t - k) \tag{15}$$

where $\{L_k\}$ and $\{H_k\}$ are pairs of discrete low-pass and high-pass filters that have the following relationship:

$$H_k = (-1)^{k-1} L_{-(k-1)} \tag{16}$$

In multi-resolution wavelet decomposition the $\{L_k\}$ plays the role of weighting function and the $\{H_k\}$ is used to compute the detailed information. The multi-resolution analysis of $L^2(R)$ is induced by dilations and translations of the scaling function

$$\varphi_{m,n}(t) = 2^{m/2}\varphi(2^m t - n) \tag{17}$$

i.e. a nested sequence of closed subspaces [14-17],

$$\Lambda \subset V_{-1} \subset V_0 \subset V_1 \subset V_2\Lambda \tag{18}$$

such that, (a) the intersection of sequence V_m has only the zero signal, i.e.,

$$I_m V_m = \{0\} \tag{19}$$

where V_m is the subspace spanned by $\{\varphi_{m,n}(t)\}_{n=-\infty}^{n=\infty}$; (b) Any signal in L^2 can be approximated by signals in the union of the spaces, V_m, i.e.,

$$\lim_{m\to\infty} V_m = L^2(R) \tag{20}$$

In addition, V_m and W_m are related by the following recursive equation

$$V_{m+1} = V_m \oplus W_m \tag{21}$$

which also implies that W_m is an orthogonal complementary space of V_m in V_{m+1} and covers the entire signal space [22].

3.2 Wavelet expansion of signal and digital filter banks

The subspaces of equation (13) give a direct-sum decomposition in $L^2(R)$, in the sense that every signal $s(t)\varepsilon L^2(R)$ has a unique decomposition. Based on the multi-resolution analysis theory of section 3.1, any signal $s(t)\varepsilon L^2(R)$ can be represented as

$$s(t) = \sum_{m,n} < s(t), \psi_{m,n}(t) > \psi_{m,n}(t) \tag{22}$$

where $< ., . >$ represents the inner product. The $s(t)$ can be approximated in a subspace V_m in the multi-resolution analysis as

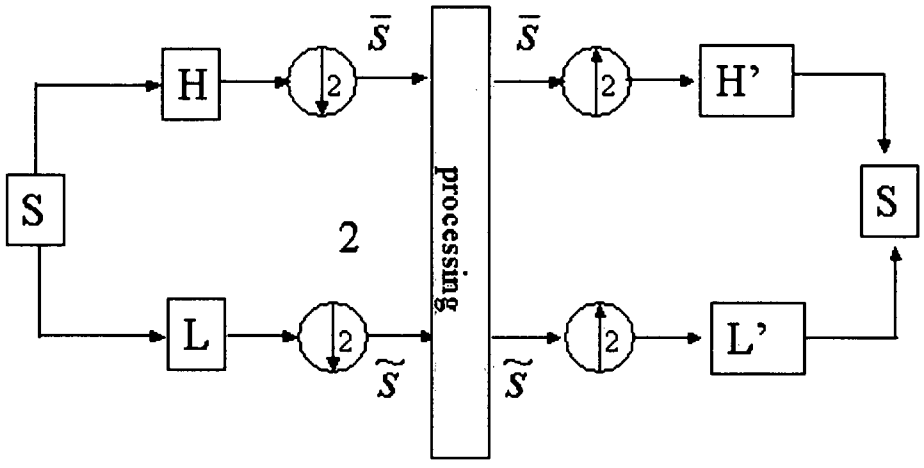

Figure 1: *Two channel filter bank. H and L form a decomposition filter bank. H' and L' form a synthesis filter bank.*

$$s(t) \cong \sum_{m,n} \bar{s}_{m,n}\varphi_{m,n}(t) \equiv A_m s(t) \tag{23}$$

where A_m is the corresponding "approximation operator" and $\bar{s}_{m,n}$ is the inner product of $s(t)$ and $\varphi_{m,n}(t)$ [25].

Using $V_m = V_{m-1} \oplus W_{m-1}$, equation (21) may be rewritten as follows

$$s(t) \cong A_m s(t) \tag{24}$$

$$s(t) = \sum_{n} \bar{s}_{m-1,n}\varphi_{m-1,n}(t) + \tilde{s}_{m-1,n}\phi_{m-1,n}(t) \tag{25}$$

$$s(t) = A_{m-1}s(t) + D_{m-1}s(t) \tag{26}$$

where D_{m-1} is the corresponding approximation operator for W_{m-1}, while $\bar{s}_{m-1,n}$ is the inner product of $s(t)$ and $\psi_{m-1,n}(t)$. In this equation, $A_{m-1}s(t)$ and $D_{m-1}s(t)$ are the low- and high- frequency components (detailed information) of $A_m s(t)$ because $\varphi_{m-1,n}(t)$ is a low-pass filter and $\psi_{m-1,n}(t)$ is a high-pass filter. The above analysis shows that the selection of a desired scaling function and mother wavelets may be reduced to the design of low-pass and high-pass filters of a two channel digital filter based on the equations (14) and (15). Consequently, the wavelet transform can be

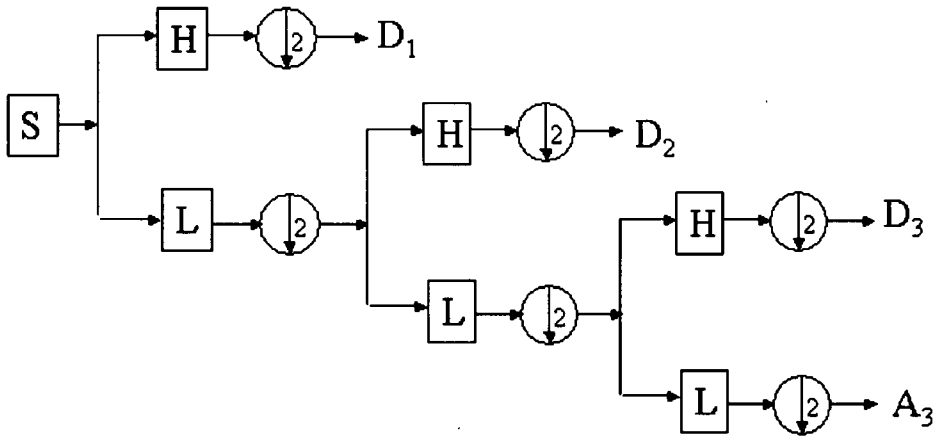

Figure 2: *The tree of filter banks for computing the discrete wavelet transform.*

simply performed by wavelet digital filter banks as shown in the left part of Figure 1 [22-24]. In the right part of the Figure 1 reconstruction is performed by a reverse procedure (from $\bar{s}_{m-1,n}$ and $\tilde{s}_{m-1,n}$ to $s(t)$). In this paper, a three level decomposition tree is applied to represent a returned radar signal, as shown in Figure 2. The results show that three-level decomposition and reconstruction is sufficient to extract m-D features. To compute the discrete wavelet transform, the low-pass bands are split, filtered and decimated. The D_1, D_2, and D_3 are the outputs from the high-pass filters (detailed information of a signal). The decomposed components may also be reconstructed by an inverse transform. During this reconstruction process, only the coefficients that are related to m-D features of the signal are used while the other coefficients are set to zero. The same process may be used to extract the stationary part of the target's body or a stationary point scatterer from a rotating part.

4. Data Description

We demonstrate the application and effectiveness of the micro-Doppler analysis with simulated and measured experimental radar data. It should be emphasized that although the theoretical results in section 2 and the proposed method given in section 3 have been demonstrated to HRR and ISAR simulated data and HRR experimental data, the m-D features can be extracted from any microwave radar system that has good Doppler resolution.

4.1 Simulated Data

4.1.1 HRR Data

There are a number of radar techniques that can be applied Automatic Target Recognition (ATR) and Non-Coorperative Target Recognition (NCTR). The radar echo provides a target profile that serves as a "signature" for identification purposes. Among some of the more promising methods are High-Range Resoulution (HRR) and Inverse Synthetic Aperture Radar (ISAR).

HRR offers a simple and rapid way to characterize an air target through the use of radar range profiles; this range profile is essentially a 1-D radar image of the target. It has an all aspect capability. It requires a modest signal to noise ratio. This technique is applicable to a wide range of a new generation of ground, naval and airborne radars [37]. The HRR profiles are simulated using an X-band stepped frequency waveform (SFWF) radar illuminating four scatterers. In this simulation, the radar operates at frequencies from 8.9 to 9.4 GHz, providing 500 MHz bandwidth. The large bandwidth is achieved synthetically by stepping through a band of frequencies. The frequency step size of 1 MHz is used. For a frequency step size of 1 MHz, it takes 500 frequency steps to provide a 500 MHz bandwidth. The maximum rate of the frequency step change of 1 kHz is used. Thus it requires 0.2 s to generate a single HRR profile, i.e., an effective HRR PRF of 5 Hz. In this simulation, the test target is made up of four point-scatterers, three scatterers of which are stationary to provide a geometric reference and a contrast to a vibrating scatterer in HRR profiles. The vibrating scatterer generates the m-D phenomenon in the radar signal. By increasing the vibration rate, the limitation of the proposed method to extract m-D features from HRR systems at this operating frequency can be studied. The vibration rate is increased from 10 to 100 Hz. The displacement of the vibration is 25 mm. The results are presented in section 5.

4.1.2 ISAR Data

ISAR is a NCTR technique that is currently being investigated for target identification by the combat ID community. ISAR provides a 2-D radar image

of a moving target [5, 6, 18]. A 2-D picture can potentially offer crucial distinctive information that can lead to a more accurate targer identification.

In this simulation, radar operates at a center frequency of 9.95 GHz and has a 300 MHz instantaneous bandwidth. The radar employs a CW, FM-modulated pulse compression waveform operating at a PRF of 2 kHz. The radar data has 626 range cells and 1000 cross range cells. In this simulation, there is a "T" shaped target contains 10-point scatterers that join at the location (0,0). The "T" shaped target is uniformly rotated at a constant rate of 5 degrees/second. Vibrating motion was then injected to the scatterer at (0,0). That is, in addition to uniform rotation (5 degrees/second), an additional sine wave is injected for the scatterer at (0,0). The limitation of the proposed method to extract m-D features from ISAR system can also be studied by increasing the vibration rate. The vibration rate is increased from 10 to 100 Hz. The displacement of the vibration is 50 mm. The results are presented in section 5.

4.2 Experimental Data

Experimental trials were conducted to investigate and resolve the micro-Doppler radar signatures of targets using an X-band radar. Two types of data collection were performed. The targets in these experiments are helicopter and walking men with swinging arms. For the helicopter trial, the helicopter was flying at an altitude of 200 feet. The range of the helicopter was at about 2.5 km. The integration time of the data collected is 96.5 ms.

The human data used in this experiment was collected using the EARS (Experimental Array Radar System) employing a stepped frequency radar waveform [17]. The experiment was conducted with the radar operating at frequencies of 8.9 to 9.4 GHz, providing a 500 MHz bandwidth. The frequency step size was 10 MHz, and a pulse repetition frequency (PRF) of 1 kHz was used. Thus, it required 50 ms to generate a single HRR profile (i.e. an effective HRR PRF of 20 Hz). The integration time for each data set was 60 seconds.

5. Results and discussion

In this section, the results are discussed using the data described in section 4. We demonstrate that the wavelet transform is able to separate the m-D motion from other contributions. Joint time-frequency analysis, that provides the time-dependent frequency information, is used to obtain additional information about the target such as vibration rate and amplitude. After several trials and comparisons, the adaptive optimal-kernel (AOK) is chosen to analyze the data since it provides better resolution and dynamic range than others [9,19]. The vibration rate is also estimated by taking the auto-correlation of the vibrating-only component of the data. The estimated value from the auto-correlation function is compared with one from time-frequency (TF) analysis. Moreover, it may be seen that the vibration rate is estimated with higher precision after the m-D features extraction process and the estimated value is the same as the one set by the simulator.

5.1 Simulated Data

5.1.1 HRR data

Scatterer with 10 Hz vibration rate

Figure 3 shows is the magnitude of the radar return from the four scatterers. The Fourier spectrum in Figure 4 is a "range profile" where the four peaks represent the four point-scatterers located. The peak spread in the spectrum indicates that there exists a modulation due to the vibrating scatterer. Figure 5 shows the TF signature of the radar return from four scatterers, where the time-varying sinusoidal curve represents the m-D of the vibrating scatterer, while the three straight lines represent three stationary scatterers.

After several trials and simulations, a wavelet with base Daubechies 10 (db10) was selected as a suitable wavelet to generate the high-pass and low- pass decomposition and reconstruction coefficients. The three-level wavelet decomposition components of the radar return are shown in Figure 6. The approximation component is reconstructed by high scale decomposition coefficients and the rotating portion can be clearly observed. The detailed parts are reconstructed from low scale coefficients. By combining these three detailed levels, the three stationary scatterers are shown in the same TF plot (Figure 7). Note that the positions of the stationary scatterers in this Figure are the same as in Figure 5. Figure 8 contains strong m-D feature due to a vibrating scatterer. It shows sinusoidal oscillation and from the TF plot, the period of the oscillation is estimated to be about 0.101 s with a vibration rate of about 9.9 Hz. The maximum m-D frequency change is about 16.5 Hz. Hence, using the estimated value of the vibration rate, the maximum m-D frequency change and equation (7), the displacement of the vibrating scatterer is estimated to be about 27 mm. This is in reasonable agreement with the simulated set value (25 mm). The period of the vibration can also be estimated

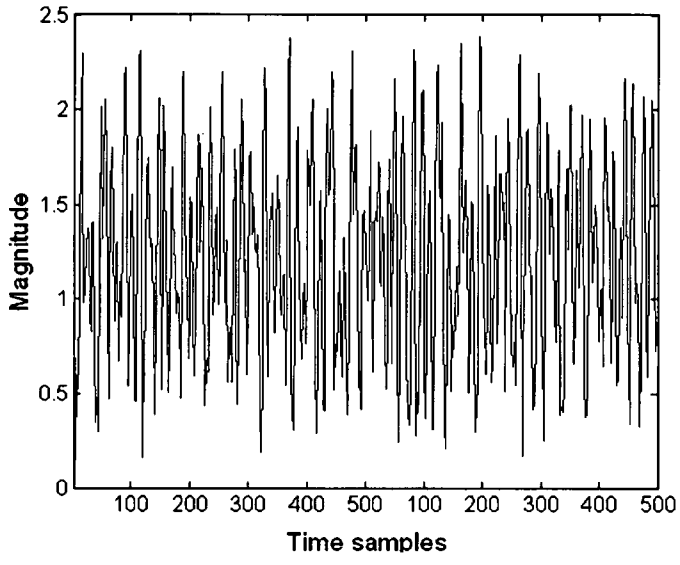

Figure 3: *The magnitude of the radar return from four point-scatterers (vibration rate is 10 Hz).*

from vibrating scatterer-only data by taking the auto-correlation of the time sequence as shown in Figure 9. The distances between the peaks in Figure 9 describe the time intervals, i.e., the period, of the vibrating scatterer. The time interval between the peaks is 100/PRF=0.1 s (since PRF=1000 Hz). Therefore the vibration rate is 10 Hz, which is consistent with the value with the TF analysis. Both estimated results agree with the simulated set value.

It should be emphasized that without using the m-D extraction process, estimating the period of the vibrating scatterer would be more difficult due to the presence of stationary scatterers. The Figure 10 shows the auto-correlation function of the unfiltered data.

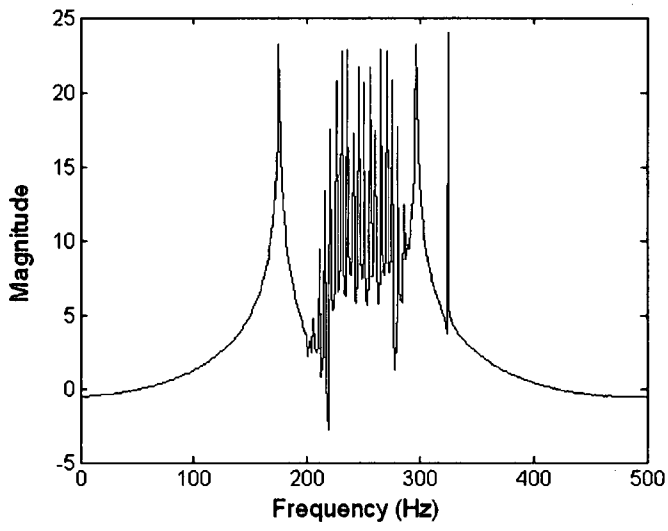

Figure 4: *The Fourier spectrum of the radar return from four point-scatterers (vibration rate is 10 Hz).*

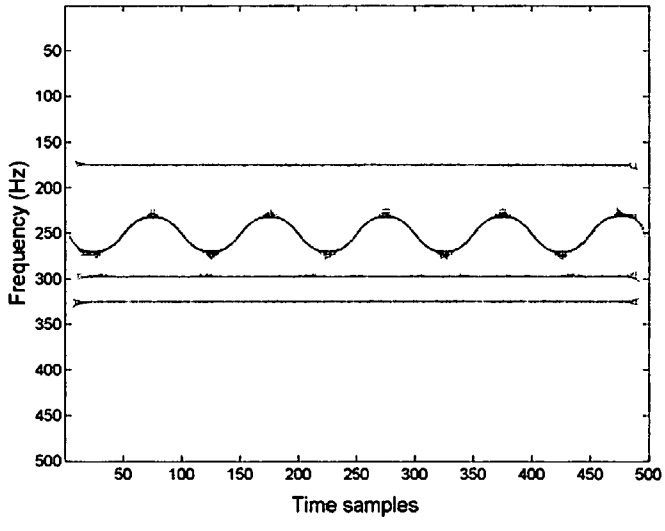

Figure 5: *The TF signature of the radar return from four point-scatterers (vibration rate is 10 Hz).*

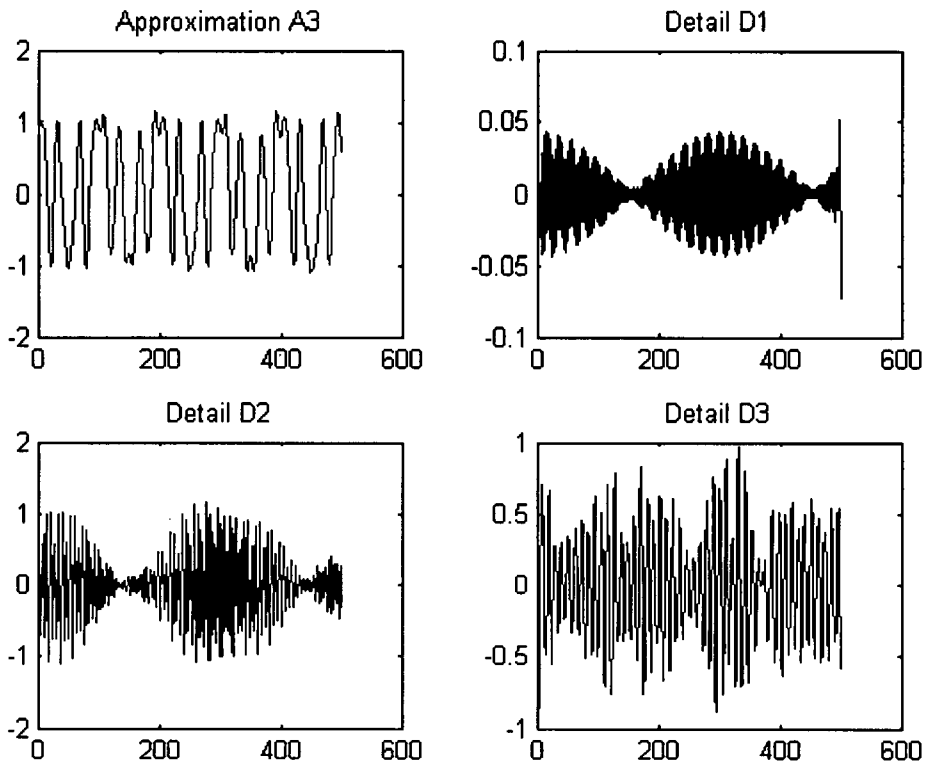

Figure 6: *The different signal components from three-level wavelet decomposition and reconstruction using digital filter bank. The horizontal axis is discrete time-samples and the vertical axis is amplitude.*

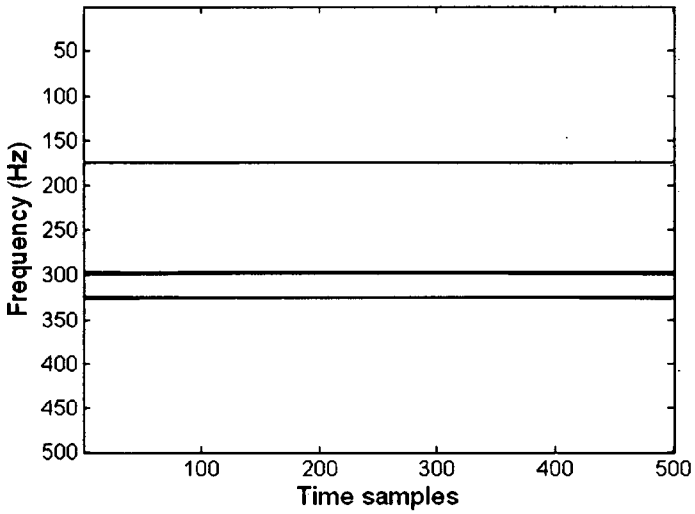

Figure 7: *TF signature of the stationary scatterers.*

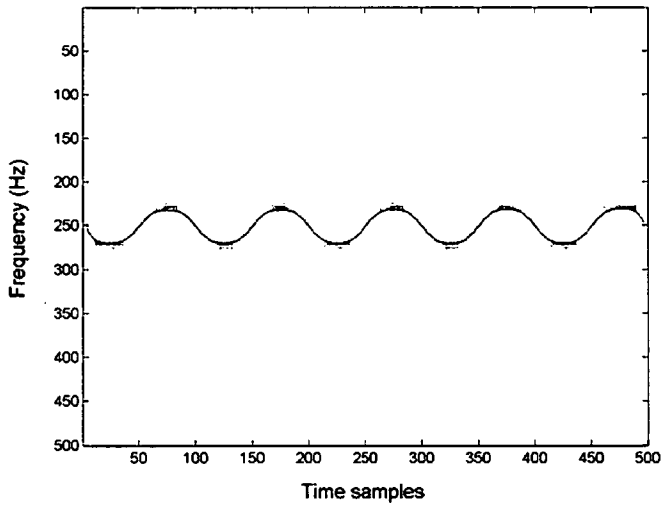

Figure 8: *TF signature of the vibrating scatterer.*

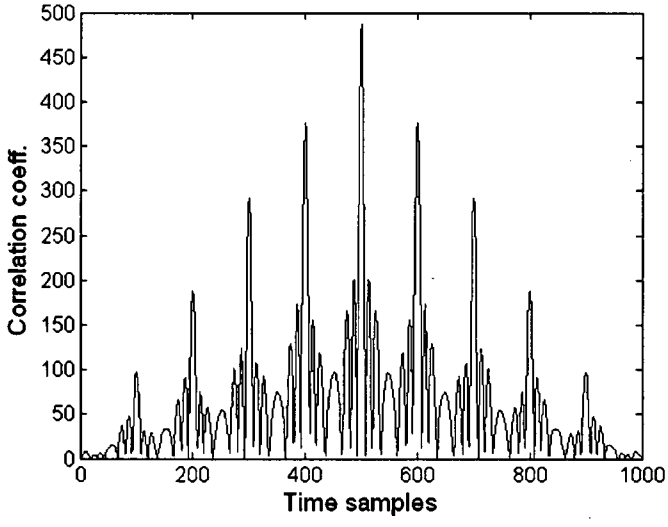

Figure 9: *The auto-correlation of the vibrating-only data.*

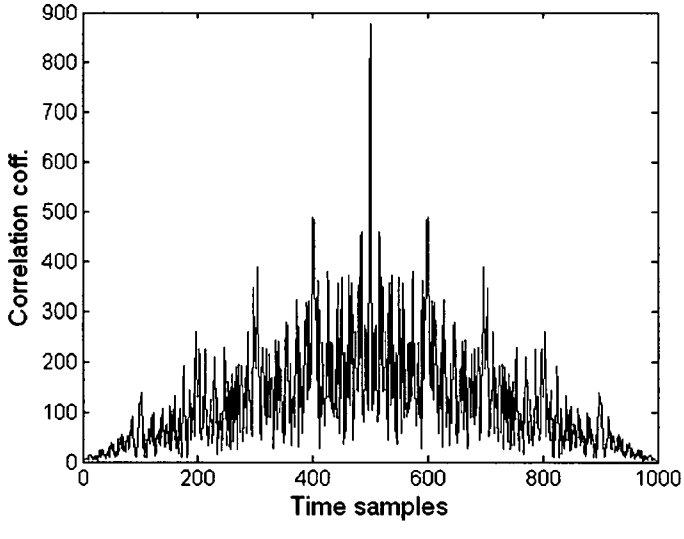

Figure 10: *The auto-correlation of the unfiltered data.*

Scatterer with 40 Hz vibration rate

The results for a vibrating scatterer with a vibration rate of 40 Hz are shown in Figures 11-16. Figures 11 and 12 show the Fourier spectrum and TF signature of the radar return from four scatterers. From Figures 11 and 12, it is impossible to identify the m-D induced by the vibrating part from that induced by the stationary part. However, they are clearly separated by using the wavelet transform method. The results for two different motion features are shown in Figures 13 and 14. In Figure 14 the m-D feature (signal) is clearly periodic and is attributed to the vibrating scatterer. The period of the oscillation is estimated to be about 0.024 s and thus the vibration rate is about 41 Hz. The maximum m-D frequency change is about 57 Hz. The maximum m-D frequency change is obtained by taking average value of maximum and minimum values due the fact that the line is not sharp in Figure 14. The corresponding displacement of the vibrating scatterer is estimated to be about 23 mm and is in reasonable agreement with the simulated value (25 mm). The period of the vibration can also be estimated from the auto-correlation function. The auto-correlation of the filtered data after m-D feature extraction is shown Figure 15. Figure 15 clearly shows the vibrating scatterer. The distances between the peaks in Figure 15 describe the period of the vibration, which is estimated to be 0.025 s. Therefore the vibration rate is 40 Hz, which is consistent with the value from the TF analysis. Both estimated results agree with the experimentally set value. The auto-correlation of unfiltered data is also shown in Figure 16. The vibration rate is difficult to accurately estimate due to a higher noise level.

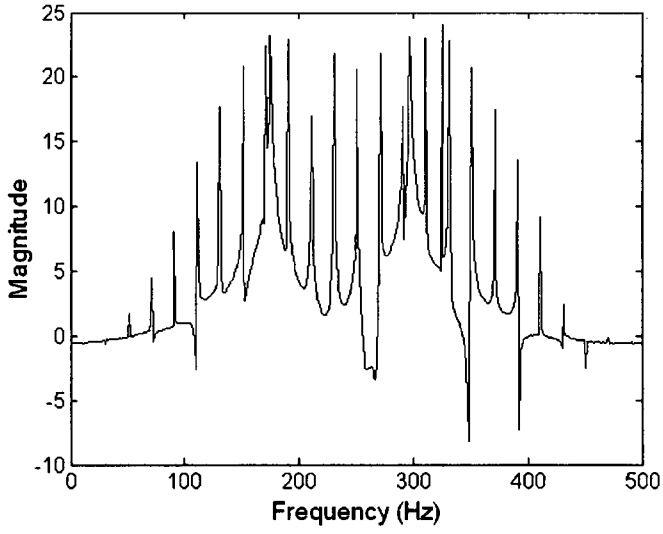

Figure 11: *The Fourier spectrum of the radar return from four point-scatterers (vibration rate is 40 Hz).*

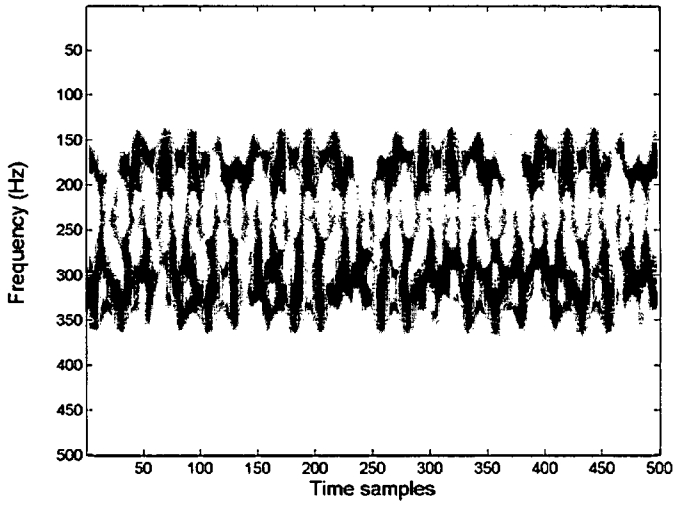

Figure 12: *The TF signature of the radar return from four point-scatterers (vibration rate is 40 Hz).*

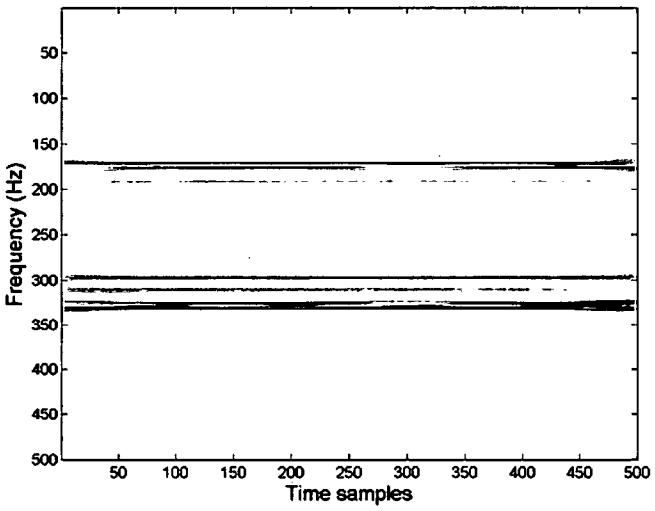

Figure 13: *TF signature of the stationary scatterers.*

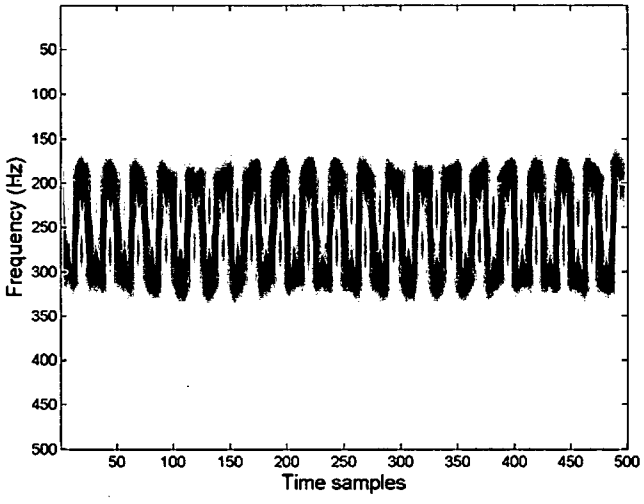

Figure 14: *TF signature of the vibrating scatterer.*

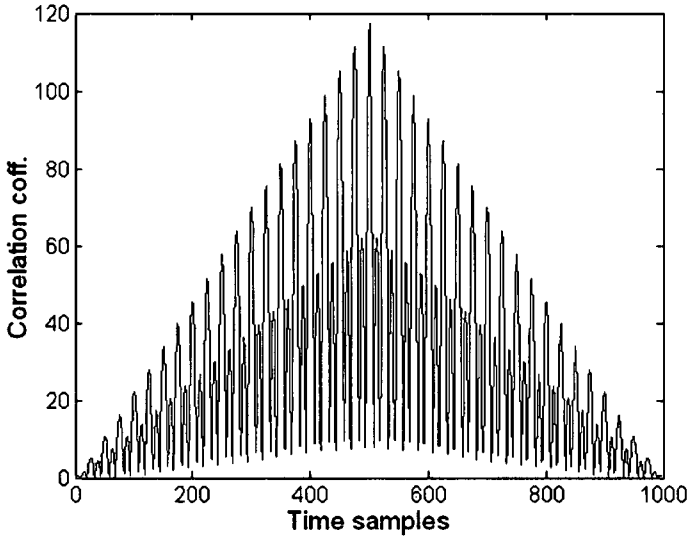

Figure 15: *The auto-correlation of the vibrating-only data.*

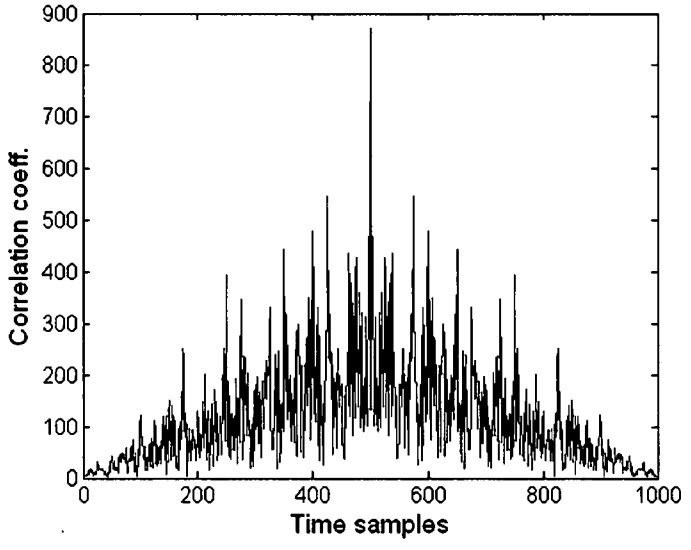

Figure 16: *The auto-correlation of the unfiltered data.*

5.1.2 ISAR data

Scatterer with 20 Hz vibration rate

A standard ISAR image of the target is obtained via the Fourier transform and is shown in Figure 17. The image in this figure is obtained by zooming in on the area where the target is located. The actual image size is 1000 cross range cells by 626 range cells. The same process is used for scatterer with a vibration rate of 40 Hz. Data between 20 and 200 range cells have been analyzed. The data in range cell 183 show a strong m-D feature. Range cell 183 of the original data corresponds to range cell 50 of the zoomed image as shown in Figure 17. The TF signature of range cell 183 in the original data is shown in Figure 18. The two motion components have been clearly shown in this figure. The horizontal trajectory around zero frequency is due to the non-vibrating scatterers of the target body, while the sinusoidal oscillation observed through the entire frequency domain is from the vibrating scatterer.

The wavelet transform outlined in section 3 is used to decompose the signal. After reconstruction, the vibrating part is separated from the target's body. In other words, the m-D feature is extracted. The results are shown in Figures 19 and 20, respectively. As it may be seen, the main features of the two returns are preserved after the decomposition and reconstruction. The Doppler features due to the vibrational motion of the scatterer are periodic. From the TF plot of m-D in Figure 20, the period of the oscillation is estimated to be about 0.0505 s and thus the vibration rate is about 19.8 Hz. The maximum m-D frequency change is about 67.5 Hz. The displacement of the vibrating scatterer is estimated to be about 50.8 mm using equation (7), and is in reasonable agreement with the simulated value (50 mm). The period of the vibration can also be estimated from vibrating scatterer-only data by taking the auto-correlation of the time sequence as shown in Figure 21. The distances between the peaks in Figure 21 describe the period of the vibration, which is estimated to be 0.05 s. The vibration rate is 20 Hz, which is consistent with the value from the TF analysis. Both estimated results agree with the simulated value. Note that without m-D extraction, it is more difficult to estimate the vibration rate from the auto-correlation function of the unfiltered data as shown in Figure 22. The peaks are much less prominent due to a higher interference level.

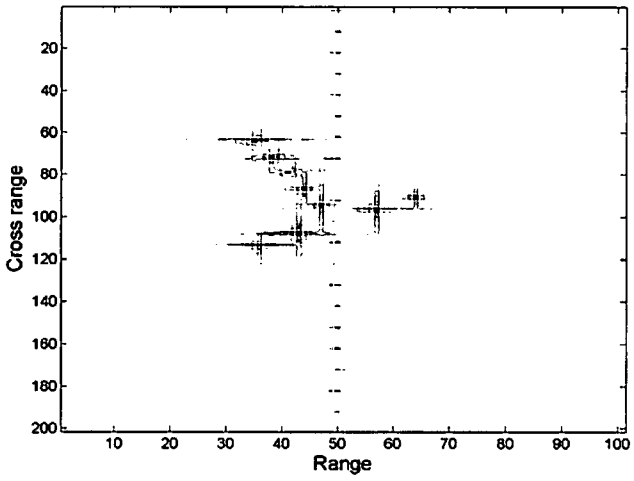

Figure 17: *ISAR image obtained via Fourier transform (vibration rate is 20 Hz).*

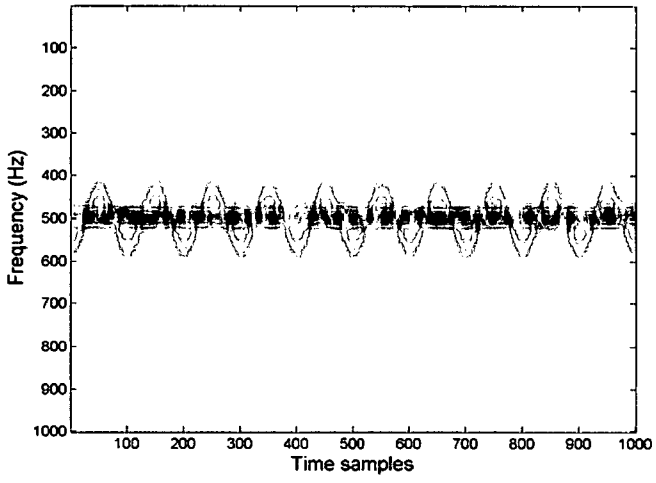

Figure 18: *The TF signature of radar return in the range cell 183 of the original data.*

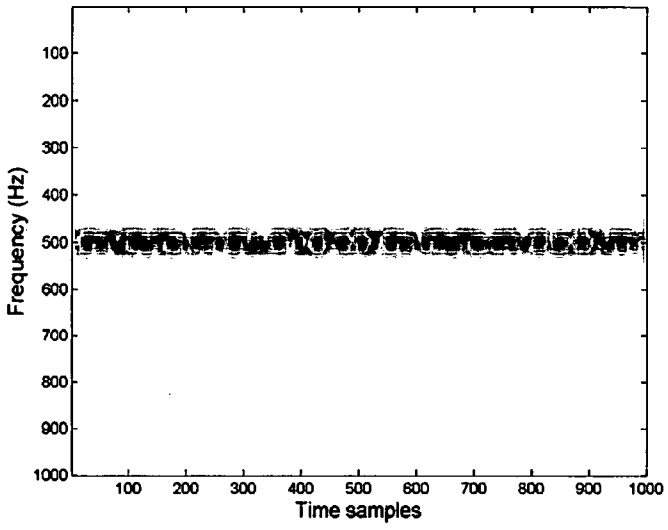

Figure 19: *The TF signature of the target body.*

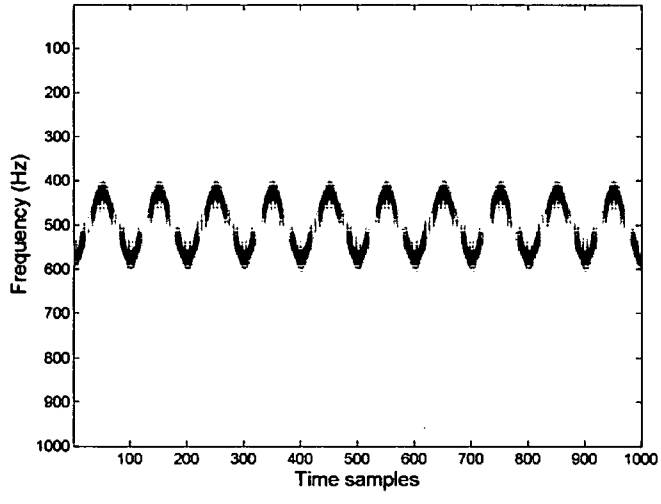

Figure 20: *The TF signature of the vibrating scatterer.*

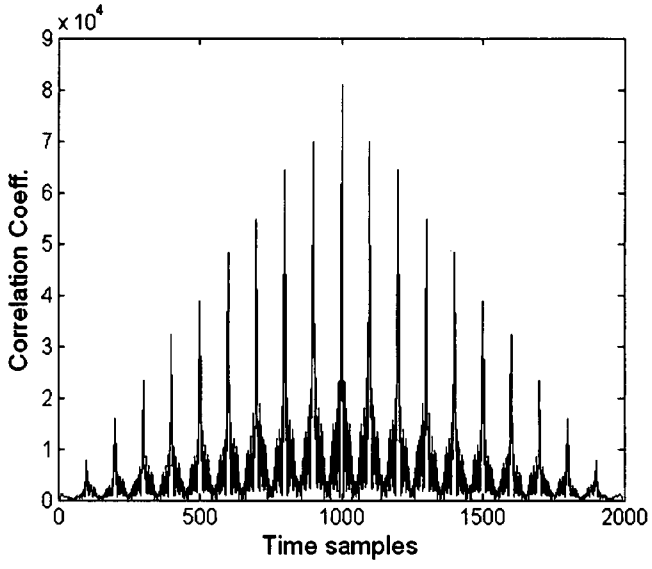

Figure 21: *The auto-correlation of the vibrating-only data.*

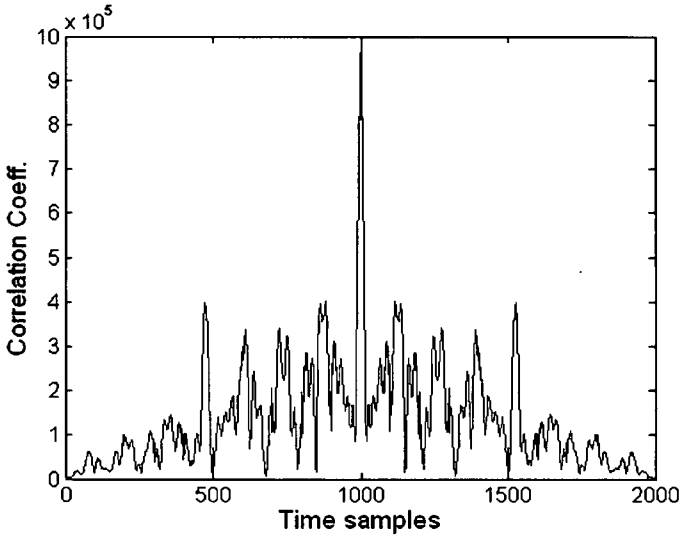

Figure 22: *The auto-correlation of the unfiltered data.*

Scatterer with 40 Hz vibration rate

The vibration rate is increased to 40 Hz. The results are shown in Figures 23-28. Figure 23 shows the standard ISAR image via the Fourier transform, while the Figure 24 shows TF signature of range cell 183 of the original data. The separation results from two different motion features are shown in Figures 25 and 26. The Doppler feature is periodic, while the period of the oscillation that is obtained from the TF plot is about 0.025s and thus the vibration rate is 40 Hz. The maximum m-D frequency change is about 130 Hz. The displacement of the vibrating scatterer is estimated to be about 49 mm and it is in reasonable agreement with the simulation value (50 mm). The period of the vibration is also about 0.025 s that is estimated by the auto-correlation as shown in Figure 27. The vibration rate is estimated to be 40 Hz. Both estimated values are consistent with simulated values. The peaks in Figure 27 are more prominent than those of Figure 28, the latter being obtained from the auto-correlation of unfiltered data.

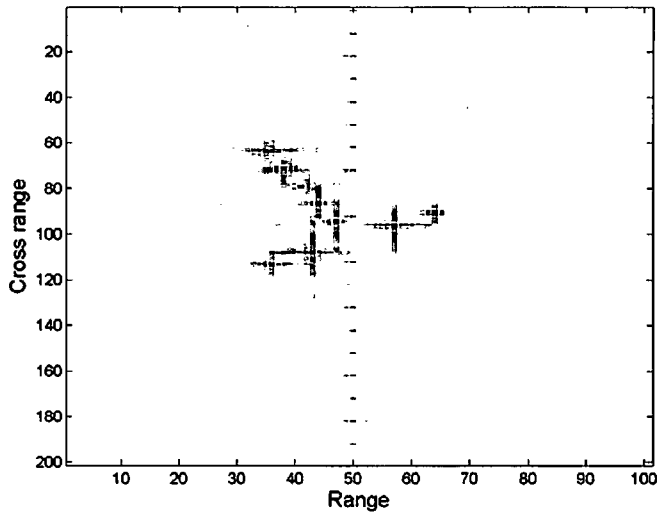

Figure 23: *ISAR image obtained via Fourier transform (vibration rate is 40 Hz).*

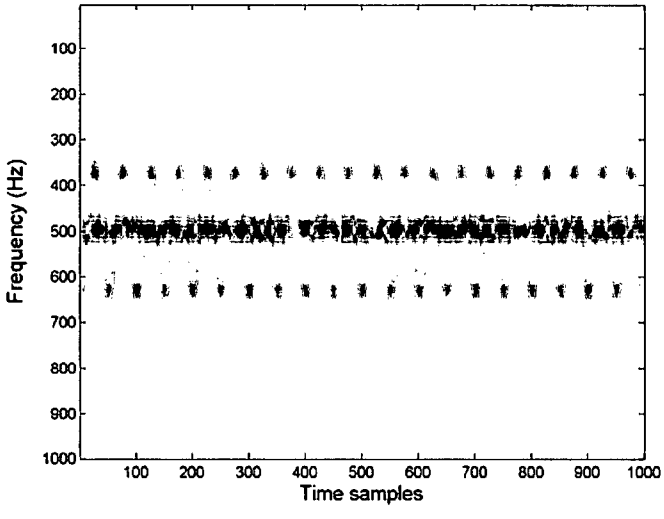

Figure 24: *The TF signature of radar return in the range cell 183 of the original data.*

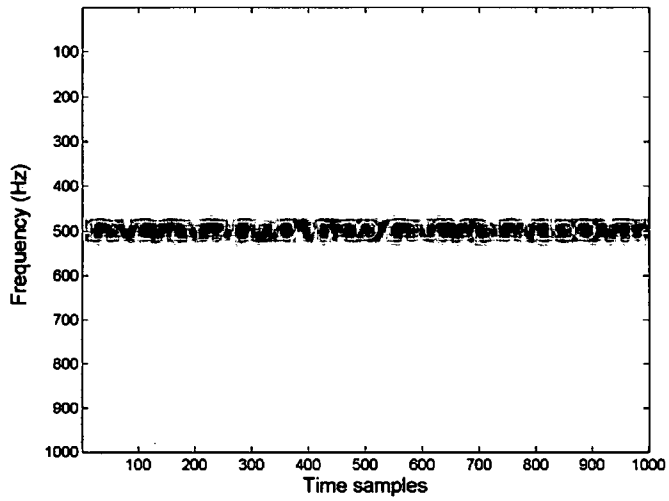

Figure 25: *The TF signature of the target body.*

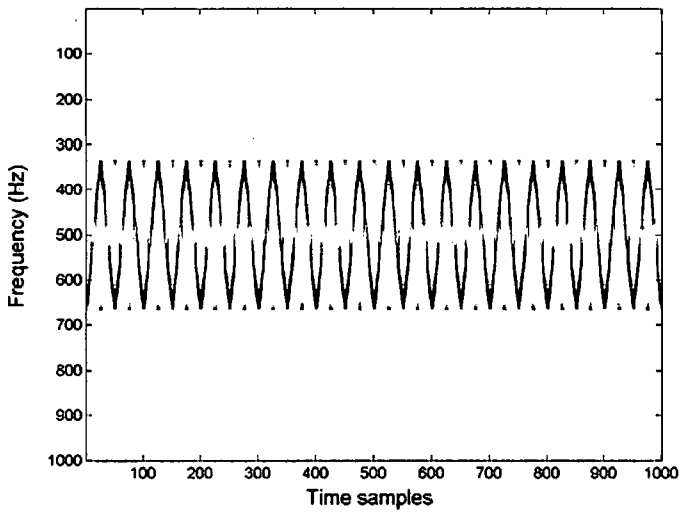

Figure 26: *The TF signature of the vibrating scatterer.*

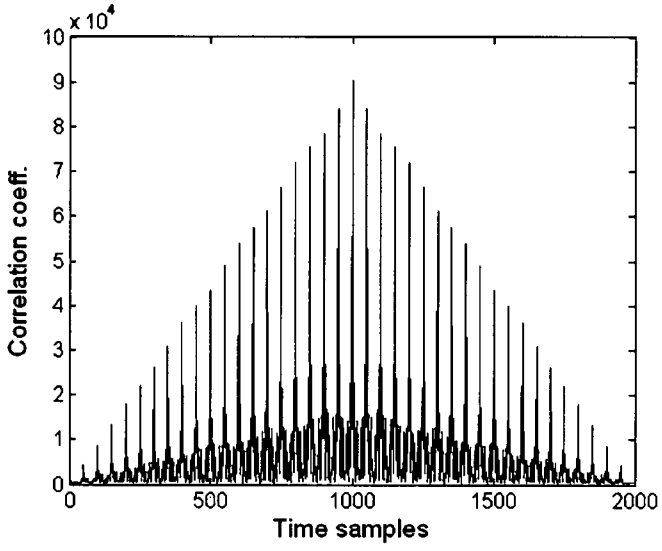

Figure 27: *The auto-correlation of the vibrating-only data.*

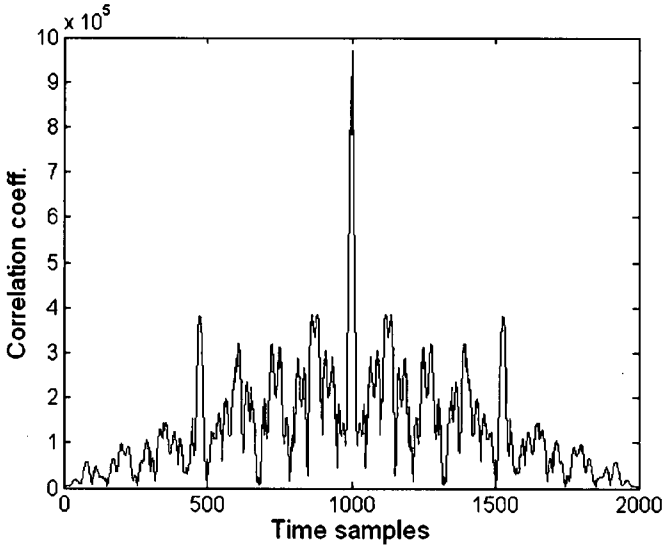

Figure 28: *The auto-correlation of the unfiltered data.*

5.1.3 Sensitivity of the wavelet-based m-D feature extraction method

In the previous sections 5.1 and 5.2, two sets of radar data are employed to demonstrate the effectiveness of the theoretical results and the proposed method. The results show that the method effectively extracts m-D features when the vibration rate is in the range of 10-40 Hz and displacement of the vibrating scatterer is in the range of 25-50 mm. Furthermore, studies for extraction of the m-D features were also performed by systematically increasing the vibration rate up to 100 Hz and applying different displacements. These studies show that the proposed method is able to extract the m-D features for vibrations lower than 100 Hz with the radar parameters specified in Table 1 and 2. For vibrations greater or equal to 100 Hz the results have many artifacts. The proposed method is not sensitive to displacement values between 5 mm and 50 mm. However, when the displacement is more than 50 mm, the wavelet decomposition level should be increased to perform m-D feature extraction.

5.2 Experimental Data

In this section we demonstrate examples of micro-Doppler signatures of targets that can be used as radar signatures for target identification. The targets in these examples are helicopter and walking man with swinging arms.

5.2.1 Helicopter Data

The experimental data used in the analysis that follows is of a hovering helicopter. For a helicopter, the main rotor blades, the tail rotor blades, and the hub have unique signatures suitable for target identification [5,38,34-36]. Generally, radar returns from a helicopter are back-scattered from the fuselage, the rotor blades, the tail blades, and the hub among other structures. The motion of the rotor blades depends upon the interdependent coupling between the aerodynamics and the rotor dynamics [4-5]. Each blade is a rotating aerofoil having bending, flexing, and twisting motion. The radar cross section of a segment of the blade depends upon its distance from the centre of rotation, its angular position, and the aspect angle of the rotor [5,34]. For simplicity, the rotor blade can be modelled as a rigid, linear, and homogeneous rod rotating about a fixed axis with a constant rotation rate.

The rotational motion of rotor blades in a helicopter imparts a periodic modulation on radar returns. The rotation-induced Doppler shifts relative to the Doppler shift of the fuselage (or body) occupy unique locations in the frequency domain. Whenever a blade has specular reflection such as at the advancing or receding point of rotation, the particular blade transmits a short flash to the radar return. The rotation rate of the rotor is directly related to the time interval between these flashes. The duration of a flash is determined by

the radar wavelength and by the length and rotation rate of the blades. A flash resulting from a blade with a longer length and a radar with a shorter wavelength will have a short duration [5].

The helicopter employed in the experiment is hovering above the ground at a height of approximately 60 m and at a range of 2.5 km from the radar. The main rotor is comprised of five blades and the tail rotor consists of six blades. The RPM of the main rotor blades is known to be 203 rpm for this helicopter. The experiment was conducted using an X-band radar. Two trials were conducted, both with an integration time of 96.5 ms.

In order to demonstrate the procedure of m-D analysis, the results for trial 1 are now presented. First, the Fourier transform of the original radar returned data is computed and the image obtained is shown in Fig. 29. As can be seen from the image, a main frequency bin with a large amplitude exists in the middle of the spectrum representing the helicopter's body vibration. Surrounding this frequency bin, one can observe two other less prominent peaks representing the frequency of the main rotor and tail rotor rotation rate. These are the m-D features that are to be extracted. By applying the wavelet analysis as described above, the m-D features are obtained. The next step in the procedure is to make use of time-frequency analysis in order to depict the m-D oscillations and to estimate the target's motion parameters. The time-frequency signature of the original returned signal using the short-time Fourier transform is given in Fig. 30. The stationary body is observed as a fairly constant signal at 0 Hz on the frequency axis. The micro-motion dynamics of the tail rotor are seen as small, quick flashes just below the constant stationary body. The micro-motions of the main rotor are visible as the three large flashes with the large period. The same time-frequency transform is applied to the extracted m-D feature representing the main rotor obtained from the wavelet analysis, and the resulting image is shown in Fig. 31. Here, not only are the flashes made clearer, but the flashes are in fact stronger peaks than those observed in the time-frequency signature of the original signal in Fig. 30. The rotation rate of the main rotor blades is calculated from Fig. 31 as follows. It is known that the main rotor of this helicopter has five blades. This is an important point as it means that the specular reflection at the advancing and receding point of rotation do not coincide with one another. Therefore, the resulting time-frequency plot will show alternating strong and weak flashes. This is indeed the case in Fig. 31. The period between the two strong flashes, i.e. the period between two blades at the advancing point of rotation, is 0.0591 s. Since there are five blades, this value is multiplied by five in order to obtain 0.2955 s, the length of time taken by a single blade to complete one full rotation. The number of rotations in one minute is given by (60 s/min)/(0.2955 s/rotation) = 203.05 rpm, which is in agreement with the actual value known to be 203 rpm. Similarly, the short-time Fourier transform has been applied to the wavelet extracted m-D

feature representing the tail rotor. Fig. 32 illustrates the end result. In this case, the flashes caused by the tail rotor have been made obvious by the removal of the stationary body and the main rotor components. Knowing that the tail rotor consists of six blades, the rotational rate of the tail rotor is measured using Fig. 32 in a similar manner as it was computed for the main rotor. The rotation rate is calculated to be approximately 1031 rpm.

The rotation rate can also be estimated by taking the autocorrelation of the time sequence data of the extracted m-D features. The autocorrelation of the original signal is given in Fig. 33. It is evident that not much information can be easily extracted from this plot. However, looking at the plots of the autocorrelations for the extracted m-D features of the main rotor and tail rotor obtained using the wavelet decomposition method in Fig. 34 and Fig. 35 respectively, the oscillations are unmistakable. The distances between the peaks describe the period of the rotation, which in turn allow one to estimate the rotation rate. Using Fig. 34, the RPM of the main rotor blades is calculated to be 203 rpm, which is consistent with the value from the time-frequency analysis. Both results agree with the actual value. Note that without m-D extraction, it is more difficult to estimate the rotation rate from the autocorrelation of the original data as shown in Fig. 33. The peaks are much less prominent due to higher interference. The signal to noise ratio (SNR) is significantly enhanced after m-D extraction as compared to the original data.

Similar results are obtained in trial 2. Fig. 36 gives the time-frequency signature of the original radar returned data. Fig. 37 shows the extracted m-D features representing the main rotor, while Fig. 38 shows those representing the tail rotor. A scenario similar to trial 1 is seen, where the plots after m-D extraction provide a much higher SNR and give clearer results. The rotation rate of the main rotor blades is calculated using the time-frequency plot of Fig. 37 to be 203 rpm. The rotation of the tail rotor blades is calculated to be 1025 rpm.

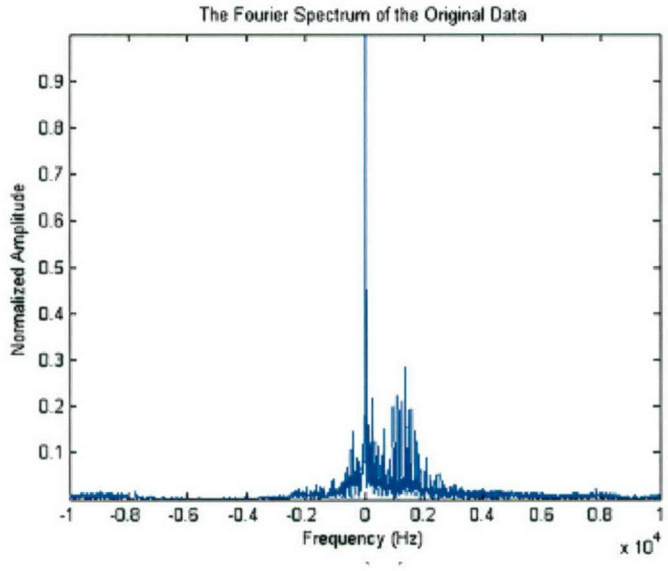

Figure 29: *The Fourier spectrum of helicopter trial 1*

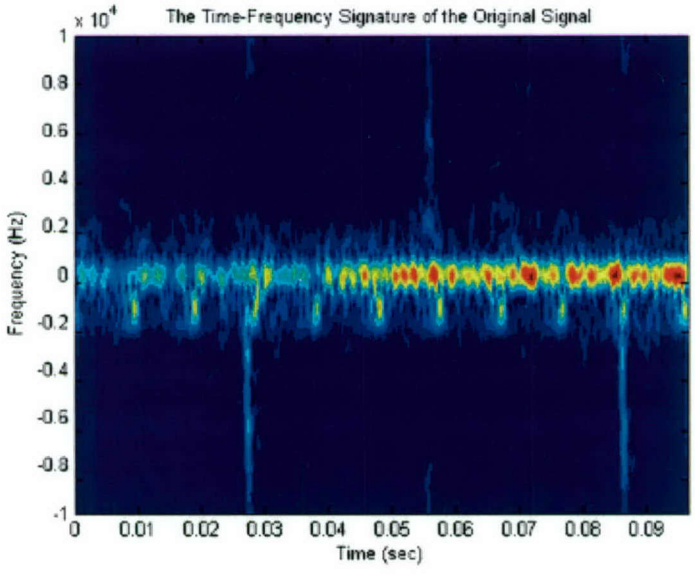

Figure 30: *The TF Signature of the original data from helicopter trial 1*

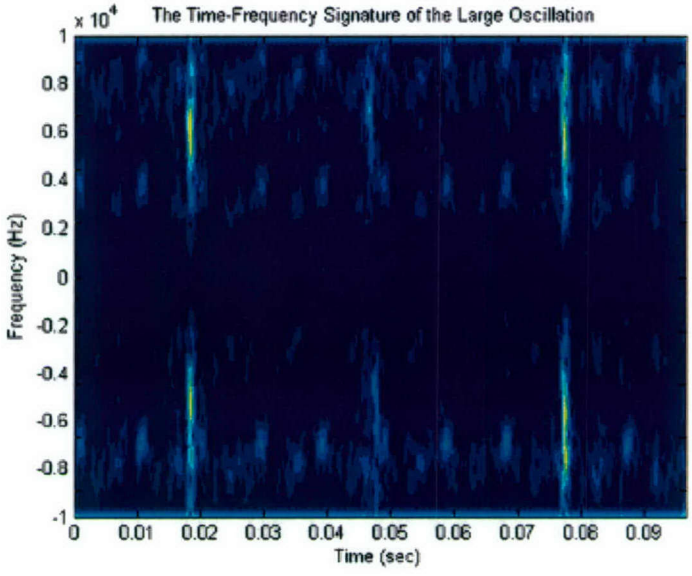

Figure 31: *The TF signature of the extracted large oscillation from helicopter trial 1*

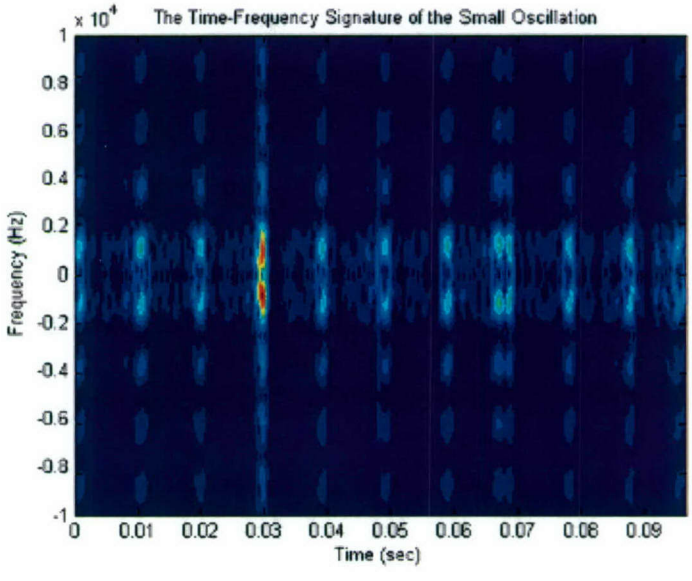

Figure 32: *The TF signature of the extracted small oscillation from helicopter trial 1*

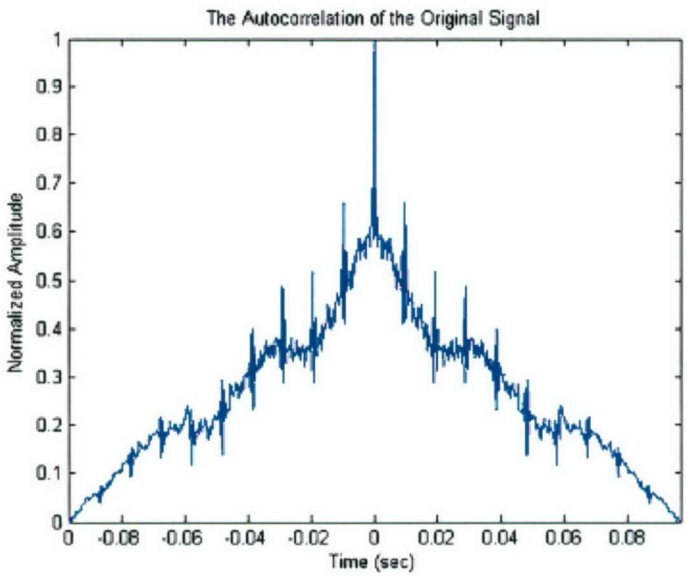

Figure 33: *The autocorrelation of the original data from helicopter trial 1*

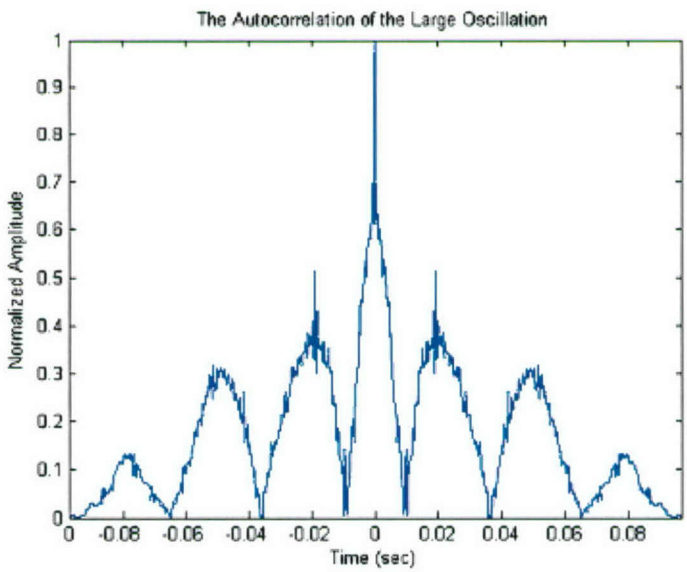

Figure 34: *The autocorrelation of the extracted large oscillation from helicopter trial 1*

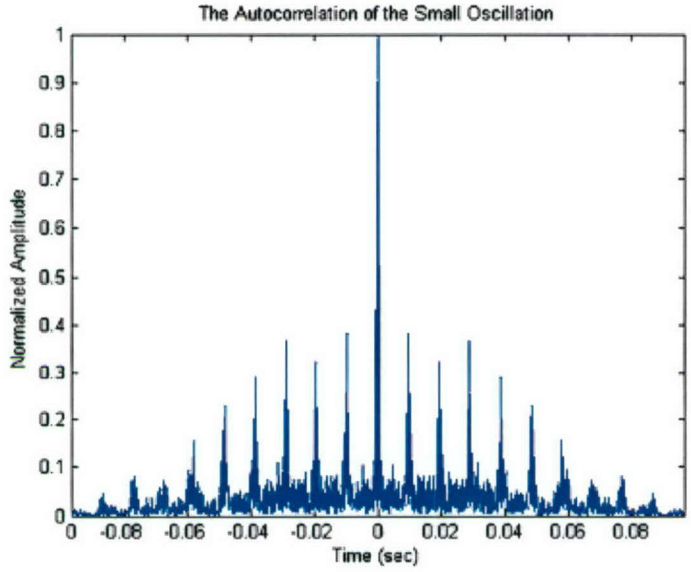

Figure 35: *The autocorrelation of the extracted small oscillation from helicopter trial 1*

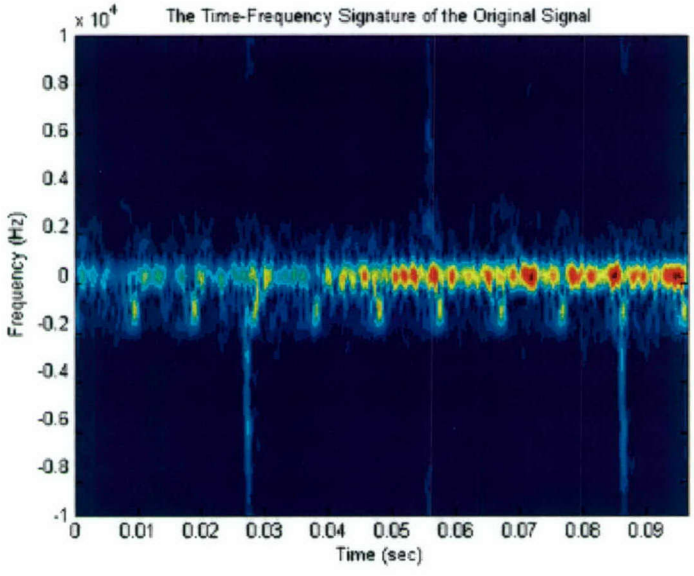

Figure 36: *TF Signature of the original data from helicopter trial 2*

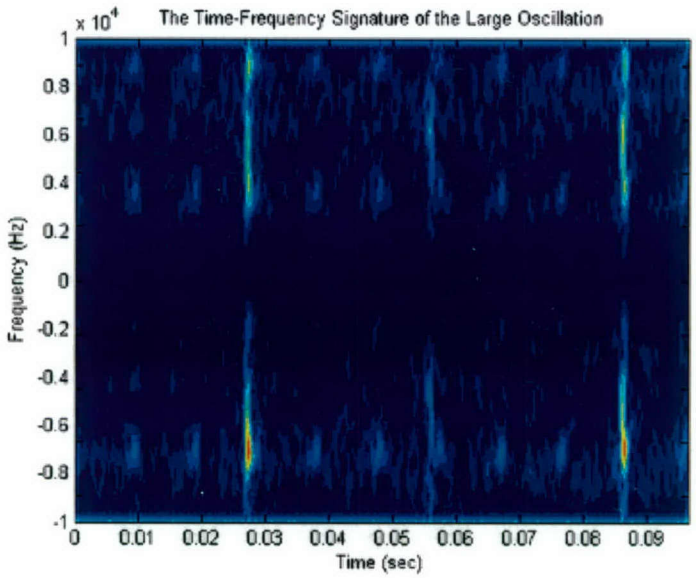

Figure 37: *The TF signature of the extracted large oscillation from helicopter trial 2*

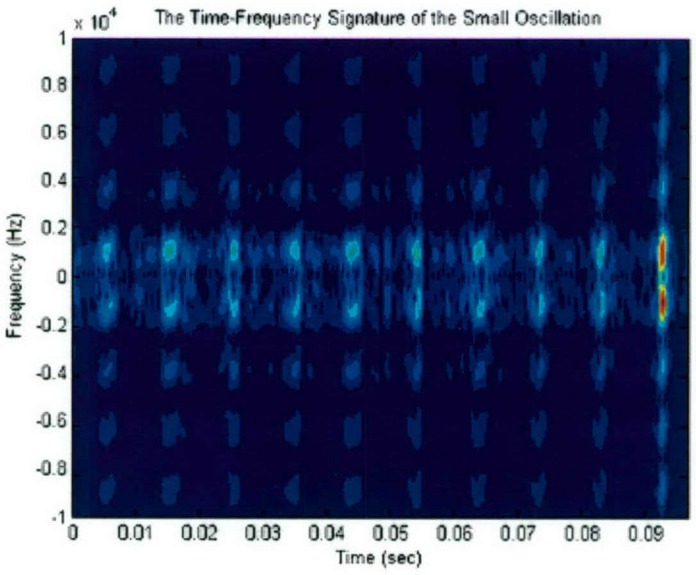

Figure 38: *The TF signature of the extracted small oscillation from helicopter trial 2*

5.2.2 Human Data

Experimental human data is used in the analysis that follows. The human gait is a complex motion behaviour that is comprised of the many movements of individual body parts. These moving body parts are the "structures" that exhibit unique m-D signatures suitable for target recognition. Hence, the information of interest contained in radar returns from human targets is the data representing the micro-motion dynamics of the various parts of the moving body. Since the body parts are moving at different velocities, a number of different frequency shifts will be obtained in the returned signal. Take, for example, a man walking and swinging his arms. The swinging motion of the arms may induce frequency modulation of the returned signal and generate sidebands about the body Doppler.

In particular, one would suspect that the motion of the swinging arms would cause a more prominent frequency modulation than the other components contributing to the radar returned signal due to the size and shape of the arms and the periodic nature of their motion in the walking gait. This being true, the experiment was conducted with an emphasis on the swinging motion of the human arms.

The experimental human data used in this experiment was collected using the EARS as described in section 4. The following six trials were conducted:

1) human marching on the spot at 30 degrees to the radar, swinging one arm, with a corner reflector

2) human walking at 45 degrees to the radar, swinging one arm, with a corner reflector

3) human marching on the spot at 30 degrees to the radar, swinging two arms, with corner reflectors

4) human walking at 45 degrees to the radar, swinging two arms, with corner reflectors

5) human marching on the spot at 60 degrees to the radar, swinging one arm, without a reflector

6) human marching on the spot at 45 degrees to the radar, swinging two arms, without any reflectors

Note that the integration time for each trial was 60 seconds.

As the results obtained from the human gait experiments are acquired in a slightly different manner than those from the experimental helicopter data, the means by which the findings are attained must first be explained. The data

from the radar returned signals for each trial are spread over a number of different range cells (51 range cells). In order to proceed with the m-D analysis, a single range cell from the set of 51 must be selected so as to permit wavelet and time-frequency analysis. A range cell must be chosen that best represents the m-D feature that is being extracted. In this case, the desired m-D feature is the arm swing. Thus, a range cell that captures the peaks of the arm swings (either the maximum or minimum points) should be selected so that the period of oscillation can be measured. Note that the period of oscillation of arm swings from all trials is known to be between 1.5 and 2.5 seconds. This is done deliberately in order to verify the results obtained from the experiments.

Now, the results of the experiment are presented starting with trial 1 (the human marching on the spot and swinging one arm with a reflector). The image on the left in Fig. 39 shows the time series of the radar returned data. The image on the right shows a zoomed version of the time series over the time interval that will be considered in the m-D analysis. Even in the time series plot of the original signal shown in Fig. 39, the Doppler frequency shift due to the swinging of a single arm is seen as an oscillation with the peak position of the arm swing in front of the body representing the maximum of the oscillation and the peak position of the arm swing behind the body representing the minimum. The image on the right in Fig. 39 shows six such oscillations.

As described above, a range cell is selected in order to carry on with the wavelet analysis. In this case, range cell 18 is used, and the time-frequency signature of the resulting data using the short-time Fourier transform is given in Fig. 40. Range cell 18 is chosen because the maxima of the oscillations are all situated across that range, thereby allowing the oscillations to be represented by the six observed flashes in Fig. 40. By applying the wavelet analysis as described earlier, the m-D features of the signal at the selected range are obtained. Finally, time-frequency analysis is utilized in order to depict the m-D arm swing oscillations and to estimate the human gait motion parameters. The time-frequency signature of the extracted arm swing feature using the short-time Fourier transform is shown in Fig. 41. One can see that there exists much less background noise in this image than that of the original signal given in Fig. 40. The period of the oscillation of the arm swing from the image on the right in Fig. 39 is measured to be approximately 2.1 seconds. When the measurement is made using Fig. 40 and Fig. 41 separately, the same value of 2.1 seconds is obtained.

Trial 2 is similar to trial 1 except for a small, yet important, difference. While trial 2 has the human swinging a single arm with a reflector just as in trial 1, trial 2 also includes the human physically walking (translational motion) whereas trial 1 is of the human marching on the spot. The fact that the human

has translational motion signifies that the radar return will include an additional range migration due to this motion. This is exactly what is observed in the image shown of the time-series on the left in Fig. 42. Again, the image on the right shows a zoomed version of the time series over the time interval that will be considered in the m-D analysis. In the images of Fig. 42, the frequency shift due to the swinging of the arm is visible from the oscillating flashes. The time interval under consideration contains three arm swings represented by the three shifted flashes. Here, the period of oscillation is measured to be approximately 2.5 seconds. After selecting a single range cell, wavelet and time-frequency analysis is performed on the data just as in trial 1. The time-frequency signature of the data at range cell 11 is shown in Fig. 43. Fig. 44 shows the time-frequency signature of the extracted m-D feature. Comparing Fig. 43 and 44, one observes a substantial decrease in noise after the wavelet analysis. In both Fig. 43 and 44, the average period of oscillation has been calculated to be 2.5 seconds.

Trials 3 and 4 are analogous to trials 1 and 2 except that they include the swinging of two arms as opposed to just a single arm. For trial 3 (marching on the spot, swinging two arms with reflectors), the time-series of the original radar return is given in Fig. 45 on the left while the zoomed in time interval is given on the right. In a double arm swing, the frequency shift is seen as two oscillations, one from each arm, phase shifted from one another by half the period of the oscillation of one arm; this is assuming that the maximum amplitude (strong specular reflection) of the oscillation of one arm occurs at the same time as the weak specular reflection of the other arm (peak position of the arm behind the body). This is what is observed in the image on the right of Fig. 45 where a smaller, weaker, second oscillation is visible in the middle of the larger, strong oscillation. The weaker oscillation represents the arm further away from the radar on the opposite side of the human body. Selecting a single range cell, in this case range 30, the time-frequency signature of the original data at a particular cell is shown in Fig. 46. That of the extracted m-D feature is given in Fig. 47. From all of the figures for this trial, the period of oscillation is measured to be approximately 2.2 seconds.

The same results from trial 2 are seen in trial 4. The corresponding images are given in Fig. 48, 49, and 50 with range 25 being selected as the appropriate cell. The only difference here is that twice the number of oscillations is seen in the same time interval. This is due to the fact that there are now two arms swinging. The image on the right of Fig. 48 gives an average period of oscillation of approximately 2.2 seconds. The period of oscillation as measured from the time-frequency representations of the data at a single range and after m-D feature extraction (see Fig. 49 and 50) differ slightly from what is measured from the time-series data as shown in Fig. 48. This difference is a result of the translational motion creating an additional phase shift together with the fact that a single range cell has been selected. Since the oscillations

are shifted upwards, corresponding points on different oscillations do not exist in the same range cell. Therefore, the measurements resulting from the data at a single range cell are not entirely accurate. Nevertheless, the average period of oscillation of the arm swings is calculated from Fig. 49 and 50 to be 2.6 seconds.

Trials 5 and 6 are analogous to the first two trials except that they are both conducted without using any reflectors whatsoever. The appropriate images for trial 5 (marching on the spot, one arm without reflector) are shown in Fig. 51, 52, and 53 with range cell 19 having been selected. The time-series plot shown on the right in Fig. 51 reveals three clearly distinguishable oscillations. Fig. 52 gives the time-frequency signature of the signal obtained after selecting range cell 19, and the three oscillations are evident in the three strong flashes. However, the signal is much too noisy. Wavelet analysis is performed in order to extract the m-D features, and the time-frequency signature of the resulting feature representing the arm swing is given in Fig. 53. Note the dramatic improvement of the SNR from Fig. 52 to Fig. 53. The period of the oscillation of the arm swings is measured to be 1.5 seconds from the image on the right in Fig. 51, from Fig. 52, and from Fig. 53.

Similarly, the images for trial 6 (marching on the spot, two arms without any reflectors) are given in Fig. 54, Fig. 55, and Fig. 56. Here, the time interval under consideration includes six oscillations as is visible from the image on the right in Fig. 54. Fig. 55 gives the time-frequency representation of the data at range cell 20. Again, wavelet analysis is performed in order to extract the m-D feature indicating the motion of the arm swing, and the time-frequency signature of the feature is shown in Fig. 56. The six flashes representing the six oscillations are clearly identifiable in this image. Keeping in mind that this trial includes two arms swinging, the period of oscillation of the arm swings is measured to be 1.5 seconds from the image on the right in Fig. 54, from Fig. 55, and from Fig. 56.

All of the results demonstrate that the m-D features are made substantially clearer after m-D analysis has taken place and establish that the period of oscillation of the arm swings is completely verified.

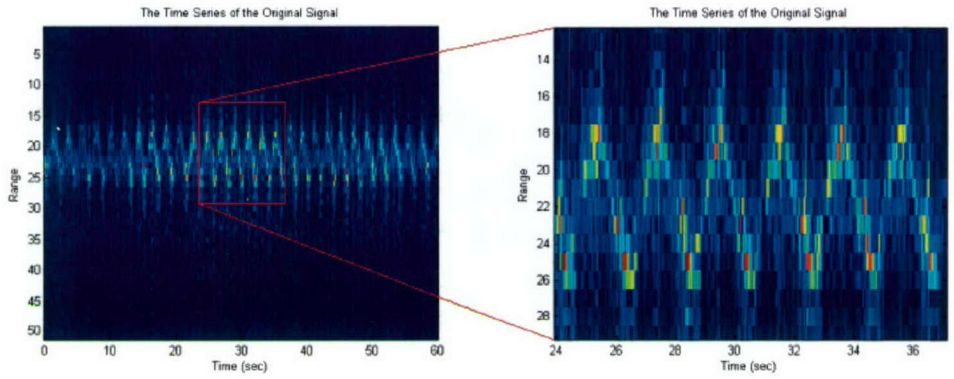

Figure 39: *The image on the left shows the time series of human trial 1. The image on the right shows the time interval under consideration for the m-D analysis*

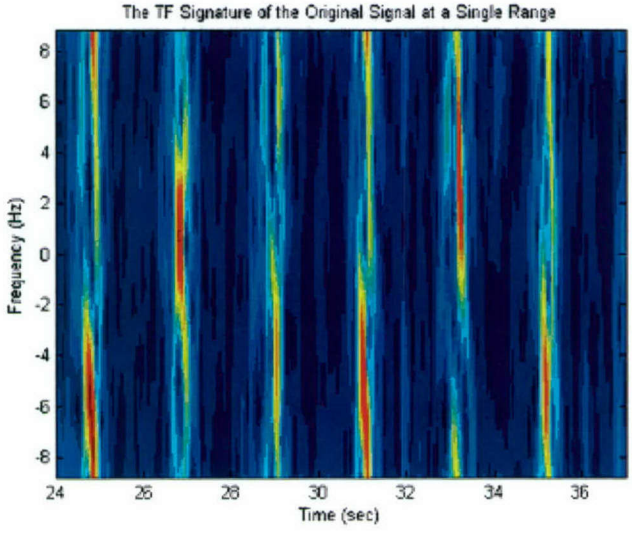

Figure 40: *The TF signature at range cell 18*

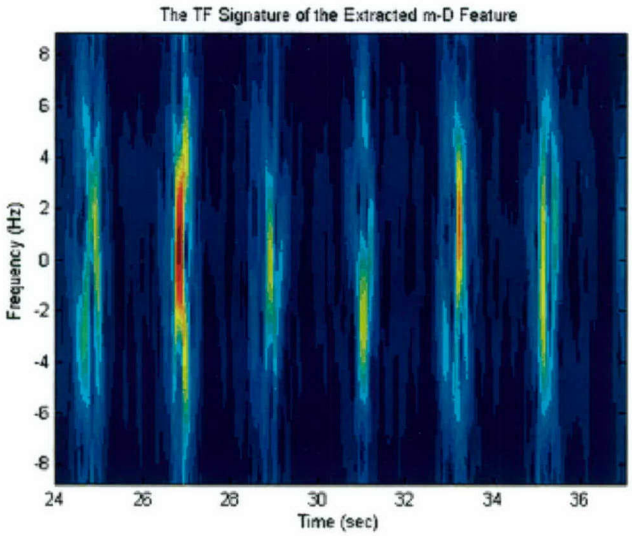

Figure 41: *The TF signature after wavelet decomposition at range 18*

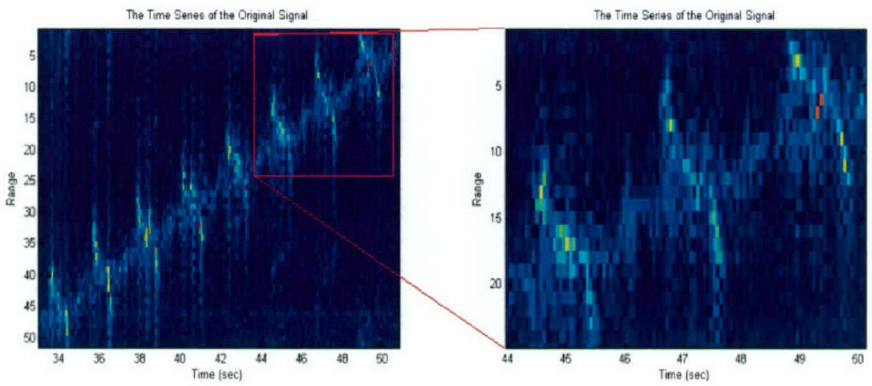

Figure 42: *The image on the left shows the time series of human trial 2. The image on the right shows the time interval under consideration for the m-D analysis*

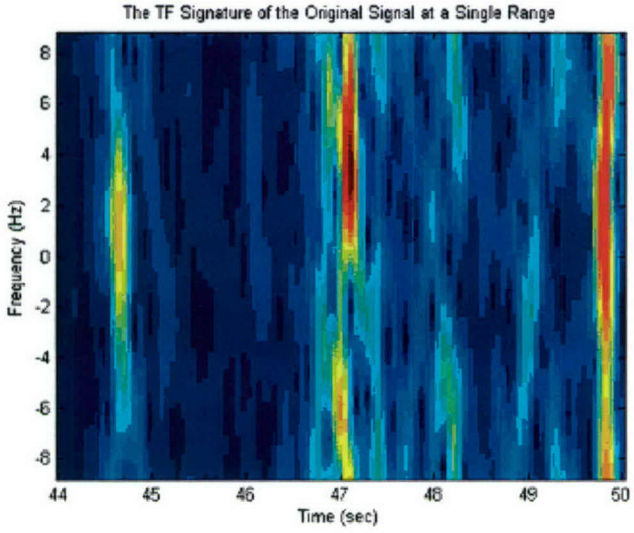

Figure 43: *The TF signature at range cell 11*

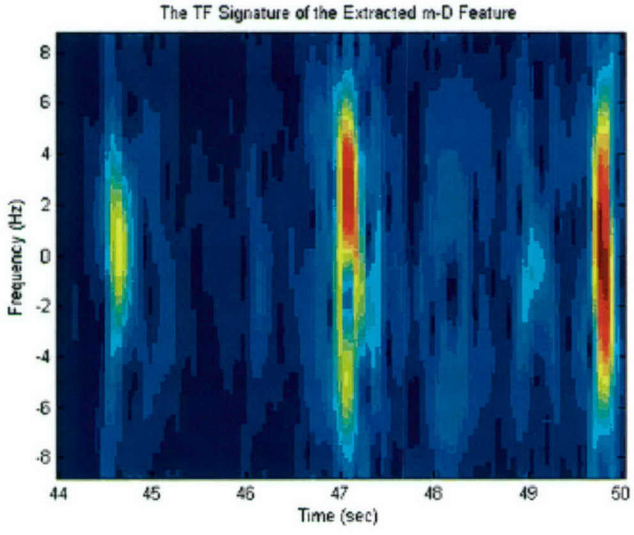

Figure 44: *The TF signature after wavelet decomposition at range 11*

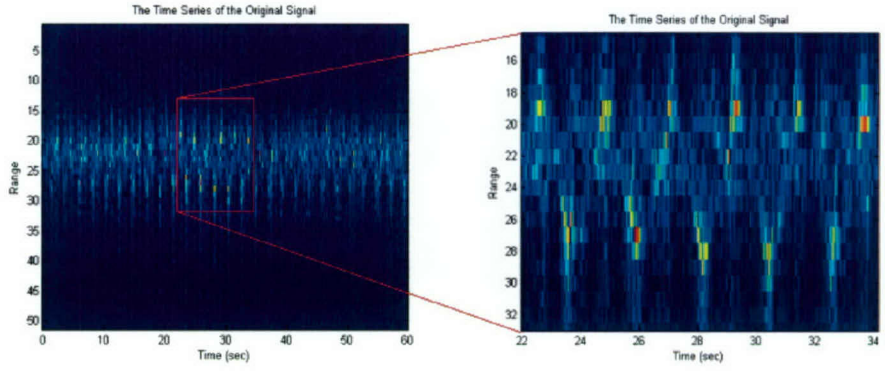

Figure 45: *The image on the left shows the time series of human trial 3. The image on the right shows the time interval under consideration for the m-D analysis*

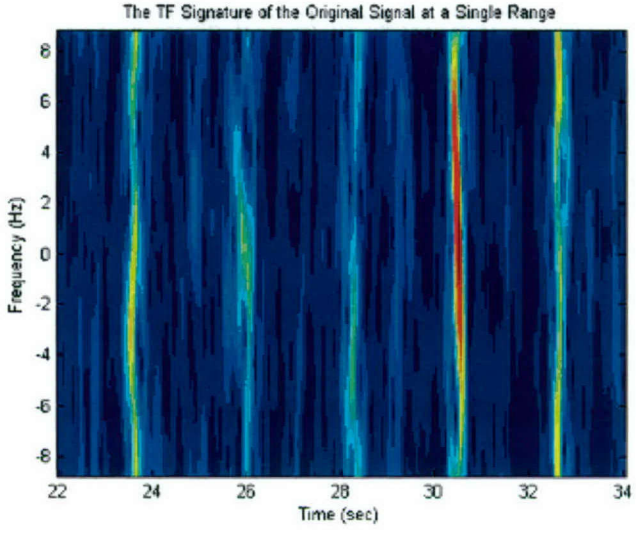

Figure 46: *The TF signature at range cell 30*

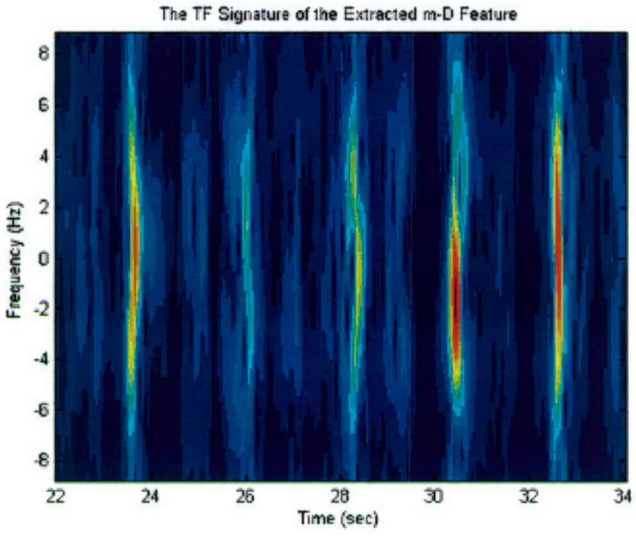

Figure 47: *The TF signature after wavelet decomposition at range 30*

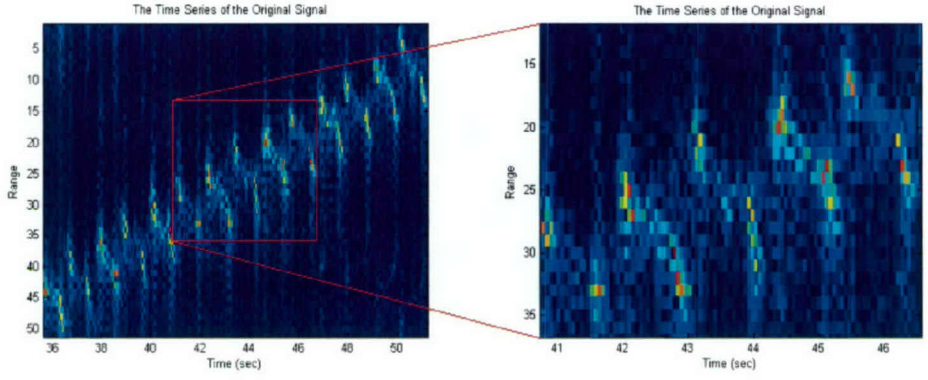

Figure 48: *The image on the left shows the time series of human trial 4. The image on the right shows the time interval under consideration for the m-D analysis*

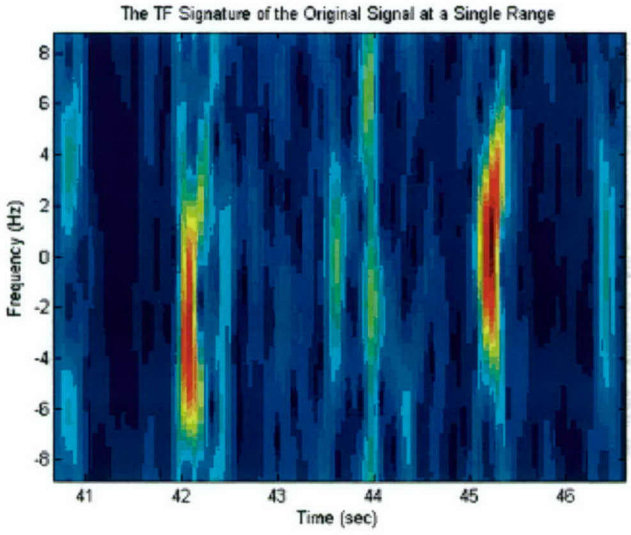

Figure 49: *The TF signature at range cell 25*

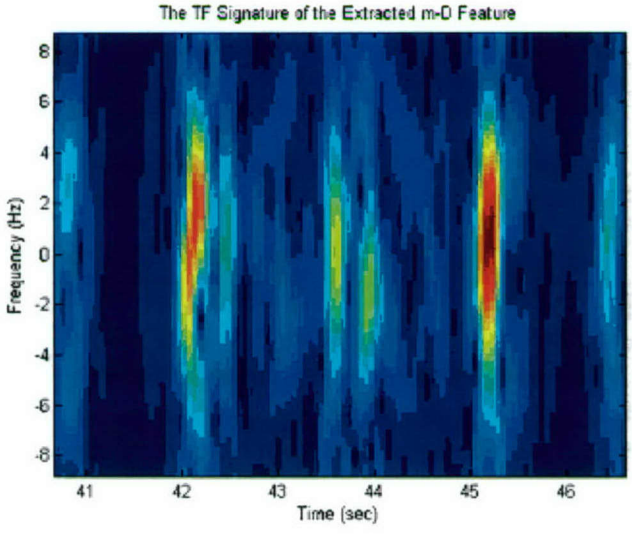

Figure 50: *The TF signature after wavelet decomposition at range 25*

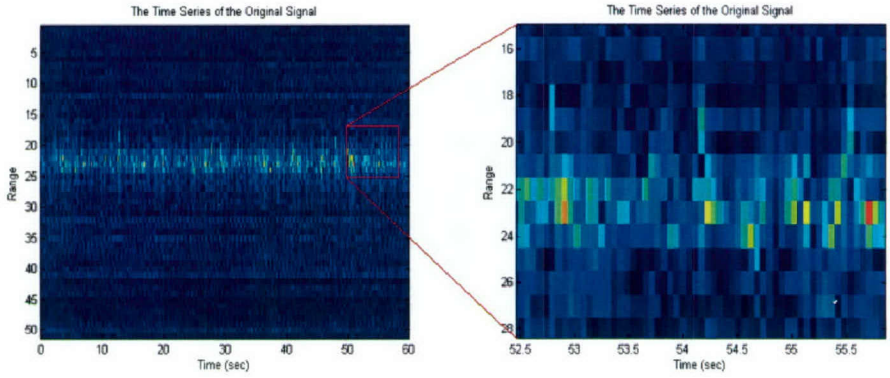

Figure 51: *The image on the left shows the time series of human trial 5. The image on the right shows the time interval under consideration for the m-D analysis*

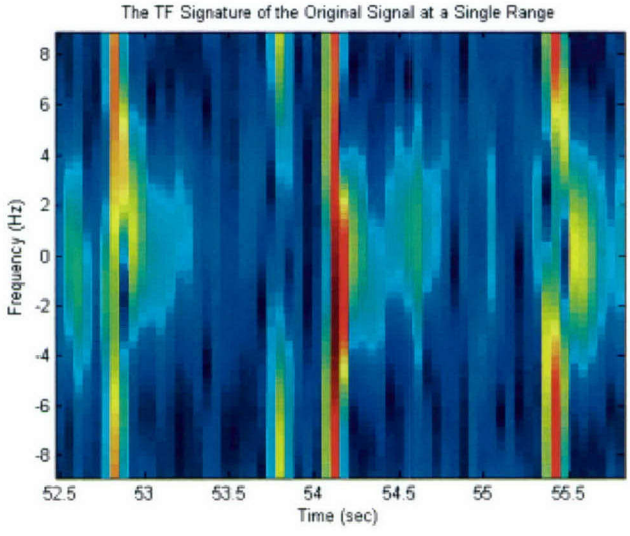

Figure 52: *The TF signature at range cell 19*

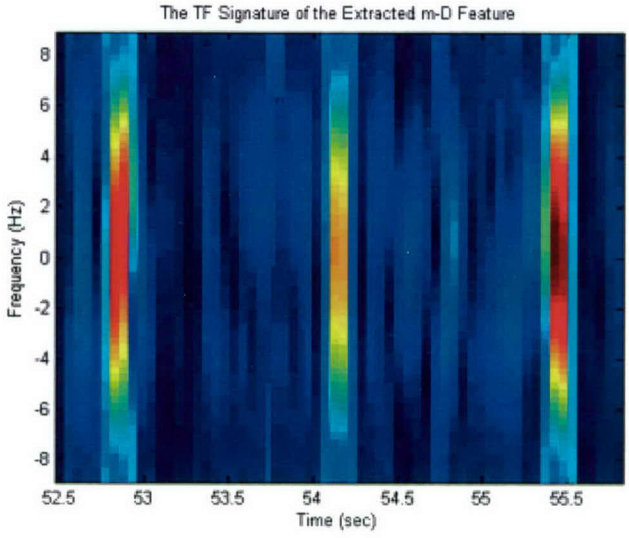

Figure 53: *The TF signature after wavelet decomposition at range 19*

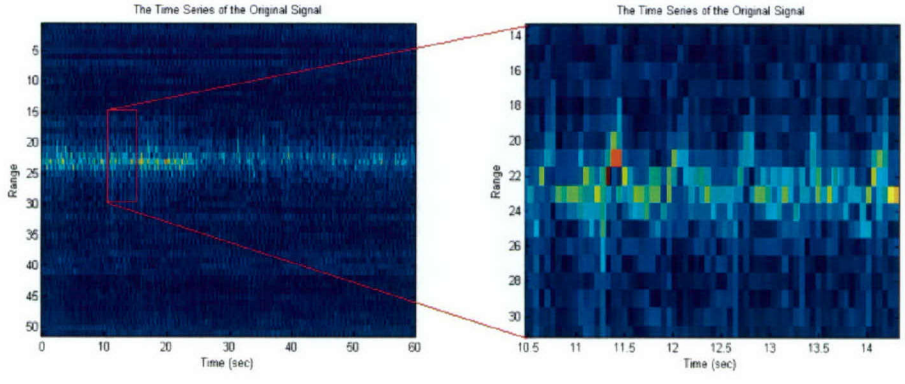

Figure 54: *The image on the left shows the time series of human trial 6. The image on the right shows the time interval under consideration for the m-D analysis*

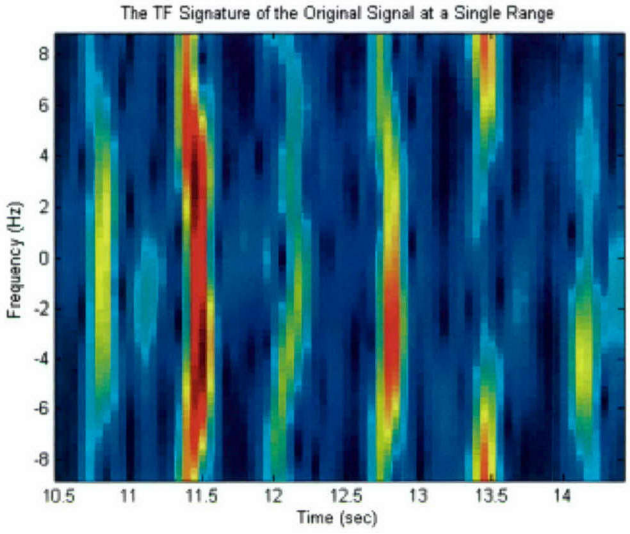

Figure 55: *The TF signature at range cell 20*

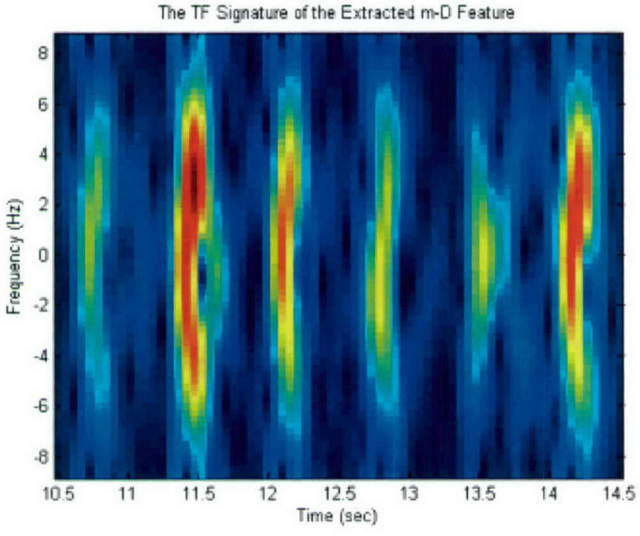

Figure 56: *The TF signature after wavelet decomposition at range 20*

6. Conclusions and Recommendations

We have shown that the vibrations or rotations of a target, or structures on a target, can induce additional frequency modulation on radar returns and generate micro-Doppler (m-D) effects. We derived mathematical formulas for m-D, and for simulated m-D signatures of targets undergoing simple sinusoidal vibration or rotation. By comparing the theoretical results with simulation results, we confirmed the accuracy of our theoretical results. From the extracted m-D signatures, the information about target's micro-motion dynamics, such as vibration rate, can be obtained.

In this report, the wavelet transform method is applied to extract micro-Doppler features from radar returns. The different signal components are obtained at different wavelet scales in the decomposition process. The extraction of m-D features is accomplished with the reconstruction process by applying the inverse wavelet transform. This methodology has been applied to simulated data with vibrational motion. The rotational motion is considered as a special case of vibrational motion. The results show that the wavelet transform methodology is an effective tool for extracting micro- Doppler features. The motion parameters of a target are accurately estimated from the extracted vibrational signal parts. The motion parameters are estimated from the time-frequency signature of the m-D and its auto-correlation. The methodology has been applied to experimental helicopter data with rotational motion and to experimental human gait data. The results show that the wavelet transform methodology is an effective tool for extracting m-D features. After the extraction of m-D features, time-frequency analysis is employed in order to estimate the motion parameters. The rotation rate of the main rotor and tail rotor blades of the helicopter is successfully computed as is the period of oscillation of the "arm-swings" of the human gait. The vibration/rotation rate of the helicopter is also estimated by taking the autocorrelation of the time sequence data. In general, it is shown that the results are much improved after the m-D extraction has taken place since only the vibration/rotational components are employed. In a future study, we intend to develop a new adaptive time-frequency and scale transform for feature extraction and recognition purpose. The investigation of different adaptive basis and mother wavelets to optimize the identification/recognition problem for military targets are a relatively new and unexplored/untested area.

The detection and extraction of m-D in radars is still immature. No known comprehensive model of m-D phenomenon applied to radar exists in open literature. Although the preliminary work on simple sinusoidal vibration or rotation has been carried out, as described in this report, there is no research available on targets undergoing complex micro-motions (real scenarios), such as a variety of non-uniform motions from the mathematical or physics points of view. A detailed study should be carried out to determine the micro-spectrum induced by complex micro-motion dynamics. The development of theoretical and numerical models of electromagnetic back-scattering from objects undergoing complex micro-motions is a new area of research.

The analysis of m-D using time-frequency techniques or wavelets is relatively new and has to be explored further. The current decomposition methods are not designed to fully represent "deep level" information from radar signatures such as the m-D effect, which affects radar Automatic Target Recognition (ATR), especially for weak moving targets buried in noise, and target returns with strong vibration or rotational components. These methods are not designed to deal with a variety of targets of interest and often do not offer the flexibility of selective feature composition during the reconstruction process (i.e., inverse transform). Therefore new algorithms, adaptive transforms and methods will have to be investigated to address these issues.

The new technology should be able to provide new capabilities for isolating unique radar return features at different decomposition levels and reconstruct selective target features by combining useful feature information from specific decomposition levels. This process should be both quick and accurate. Complete mathematical models and new software have to be developed for real-time radar military applications.

Investigation of different adaptive basis and mother wavelets to optimize the identification/recognition problem for military targets is a relatively new and unexplored/untested area. A methodology has to be researched and developed to demonstrate the capability of extracting relevant information that is embedded in both computed and measured target signatures for robust target identification in a ATR system.

Another area of high interest is the application of m-D features for AGR systems. Because gait recognition techniques is very new, researchers are still assessing the uniqueness of gait as a discriminant and methods by which it can be evaluated. Various computer vision and ultrasound techniques have been developed to measure gait parameters. Video cameras require good light and a clear view. If weather is poor or if ambient light is low, targets are unlikely to be detected, much less identified. In many theatres, this provides the enemy opportunities to move assets safely and stealthily. The greatest advantage of radar over other sensors is that it can operate effectively at all times of day and in all weather conditions. Thus radar can be used in situations where other sensors give low performance or cannot be used at all. Radar measures the direction, distance and radial velocity of the walking person as a function of time. Radar processing can reveal more characteristics of the walking human. When human body parts do not move with constant radial velocity, the m-D signatures are time-varying and therefore it is recommended time-frequency analysis techniques can be used to obtain more characteristics. However, radar-based recognition in this area is such a innovative approach that much fundamental research has yet to be done. This study gives a preliminary approach as to how to perform this work.

We recommend that a man-portable "micro-Doppler radar" be constructed for a timely, rapid and accurate response in battlefield or disaster scenarios. A high-power, coherent, wide-band radar with high-Doppler resolution is preferable. For example, when the radar frequency is at X-band or higher, the movement of a person's various body parts provides a characteristic m-D signatures. A man-portable "micro-Doppler radar" can

be used by infantry and airborne troops to detect hostile signals from battlefield or disaster areas. The compact, self-contained and flexible radar is suitable for use in mountain and highland regions. In addition, it can also be used at border sentry posts.

Acknowledgments

We would like to thank Silvester Wong (DRDC Ottawa) for his comments and suggestions for improvement of this work. We also wish to thank him for supplying us with the simulated data.

References

1. Cranos, R. (1997). Combat Identification in the future: Maintaining the Balance, *SPIE,* Vol. 3068, pp. 484.

2. Van der Heiden, R. (2000). Industry guidance for participation in the SET040 TG22 on Non-Cooperative Air Target Identification by radar, *NATO SET040 TG22,* working paper NC3A-XLVII-3.

3. Geisheimer, J.L., Marshall, W. S. and Greneker, E. (2001). A continuous-wave (CW) radar for gait analysis, *35th IEEE Asilomar Conference on Signal,* Systems and Computers, vol. 1, pp. 834-838.

4. Chen, V. C. (2000). Analysis of radar micro-Doppler signature with time-frequency transform, *Proceedings of the 10th IEEE Workshop on Statistical Signal and Array Processing,* pp. 463-466.

5. Chen, V.C. and Ling, H. (2002). Time-Frequency transform for radar imaging and signal analysis, Artech House, BOSTON.

6. Thayaparan, T., Lampropoulos, G., Wong, S. K. and Riseborough, E. (2003). Application of adaptive time-frequency algorithm for focusing distorted ISAR images from simulated and measured radar data, *IEE Proc.-Radar Sonar Navig.,* Vol. 150, No. 4, pp. 213-220.

7. Thayaparan, T. and Kennedy, S. (2004). Detection of a maneuvering air target in sea-clutter using joint time-frequency analysis techniques, *IEE Proc.-Radar Sonar Navig.,* Vol. 151, No. 1, pp. 11-18.

8. Yasotharan, A. and Thayaparan, T. (2002). Strengths and limitations of the Fourier method for detecting accelerating targets by pulse Doppler radar, *IEE Proc.-Radar Sonar Navig.,* Vol 149, No. 2, pp 83-88.

9. Thayaparan, T. and Lampropoulos, G. (2003). A New approach in time-frequency analysis with applications to experimental high range resolution radar data, *DRDC Ottawa TR 2003-187,* Defence R&D Canada - Ottawa.

10. Thayaparan, T. (2000). Linear and quadratic time-frequency representations, *DREO TM 2000-080,* Defence Research Establishment Ottawa.

11. Thayaparan, T. (2000). Limitations and strengths of the Fourier transform method to dectect accelerating targets, *DREO TM 2000-078,* Defence Research Establishment Ottawa.

12. Thayaparan, T. and Yasotharan, A. (2001). A novel approach for the Wigner distribution formulation of the optimum detection problem for a discrete-time signal, *DREO TM 2001-141*, Defence Research Establishment Ottawa.

13. Thayaparan, T. and Yasotharan, A. (2002). Application of Wigner distribution for the Detection of accelerating low-altitude aricraft using HF surface-wave radar, *DREO TR 2002-033,* Defence Research Establishment Ottawa.

14. Thayaparan, T., Lampropoulos, G., Wong, S. K., and Riseborough, E. (2003). Focusing ISAR images using adaptive joint time-frequency algorithm on simulated and experimental radar data, *DRDC Ottawa TM 2003-089,* Defence R&D Canada - Ottawa.

15. Thayaparan, T. and Kennedy, S. (2003). Application of joint time-frequency representations to a maneuvering air target in sea-clutter analysis: analysis beyond FFT, *DRDC Ottawa TR 2003-090,* Defence R&D Canada - Ottawa.

16. Thayaparan, T. and Yasotharan, A. (2001). Detection of low-altitude aircraft using time-frequency analysis for high frequency surface radar, International Radar Symposium India (IRSI-2001), Bangalore, India, December 11-14.

17. Thayaparan, T. and Stockwell, B. (2001). A comparison of time-frequency analysis techniques, International Radar Symposium India (IRSI-2001), Bangalore, India, December 11-14.

18. Thayaparan, T., Lampropoulos, G., Wong, S. K., and Riseborough, E. (2003). Adaptive joint time-frequency analysis for focusing ISAR images from simulated and experimental radar data, SPIE's 10th international symposium on remote sensing, SPIE Code Number 5238-48, September 8-12, Barcelona, Spain.

19. Lampropoulos, G., Laskin, E. and Thayaparan, T. (2002). New concepts in time-frequency estimators with applications to ISAR data, *Proceedings of SPIE,* September, Vol. 4883, pp. 27-38.

20. Cohen, L. (1995). Time-frequency analysis, Prentice Hall PTR, New Jersey.

21. A.U.G. Signals Ltd. (2002). Time-frequency algorithms for focussing distorted ISAR images, Contract No. W7714-011498/001/SV.

22. Qian, S. (2002). Introduction to time-frequency and wavelet transforms, Prentice Hall PTR, New Jersey.

23. Sheng, Y. (1995). Wavelet Transform, in the book the transforms and applications handbook. A. D. Poulariskas Ed., Chap. 10, pp. 747-827. CRC and IEEE Press, Boca Raton.

24. Strang, G and Nguyen, T. Q. (1995). Wavelet and Filter Banks, Wellesley-Cambridge Press, Wellesley, Massachusetts.

25. Mallat, S. (1989). A theory for multiresolution signal decomposition: The wavelet representation, *IEEE Trans. Pattern Anal. Machine Intell.,* Vol. 11, pp. 674-693.

26. Little, J.J. and Boyd, J. E. (1998). Recognizing people by their gait: the shape of motion, *Journal of Computer Vision Research,* vol. 1, no. 2.

27. Niyogi, S. A. and Adelson, E. H. (1994). Analyzing and recognizing walking figures in XYT, *IEEE Proceedings on Computer Vision and Pattern Recognition,* pp. 469-474.

28. Sabatini, A. M. and Colla, V. (1998). A method for sonar based recognition of walking people, *Robotics and Autonomous Systems,* Vol. 24, pp. 117-126.

29. Weir, R. F. and Childress, D. S. (1997). A new method of characterizing gait using a potable, real-time, ultrasound ranging device, *Proceedings of the 19th International Conference,* IEEE Engineering in Medicine and Biology Society, pp. 1810-1812.

30. MSTAR brochure. (2002). http://www.bluemarblegeo.com/docs/Customer-Brochures/Mstar.pdf.

31. Man-Portable Surveillance and Target Acquisition Radar (MSTAR), http://www.seistl.com/products/mss/mstar.html.

32. AN/PPS-5 MSTAR ground radar, http://www.periscope.ucg.com/mdb-smpl/weapons/sensors/grdradar/w0003502.shtml.

33. Tremblay, F. (1995). Generalization of the DREO radar jet engine modulation algorithm, DREO TR 1995-1199.

34. Martin, J. and Mulgrew, B. (1990). Analysis of theoretical radar return signal from aircraft propeller blades, *IEEE 1990 international radar conference,* pp. 569-572.

35. Misiurewicz, J., Kulpa, K., and Czekala, Z. (1997). Analysis of recorded helicopter echo, *IEE Radar 98,* Proceedings, pp. 449-453.

36. Marple, S. L. (2001). Large dynamics range time-frequency signal analysis with application to helicopter Doppler radar data, *ISPA Conference,*

37. Wehner, D. R. (1987). High Resolution Radar, Artech House, USA.

38. Wellman, R.J., and Silvious, J. L., "Doppler Signature Measurements of an Mi-24 Hind-D Helicopter at 92 GHz," ARL-TR-1637, Army Research Laboratory, Adelphi, Maryland, July 1998.

DOCUMENT CONTROL DATA

(Security classification of title, body of abstract and indexing annotation must be entered when the overall document is classified)

1. ORIGINATOR (the name and address of the organization preparing the document. Organizations for whom the document was prepared, e.g. Establishment sponsoring a contractor's report, or tasking agency, are entered in section 8.)

Defence R&D Canada – Ottawa
Ottawa, Ontario, Canada K1A 0Z4

2. SECURITY CLASSIFICATION (overall security classification of the document, including special warning terms if applicable)

UNCLASSIFIED

3. TITLE (the complete document title as indicated on the title page. Its classification should be indicated by the appropriate abbreviation (S,C or U) in parentheses after the title.)

Micro-Doppler radar signatures for intelligent target recognition (U)

4. AUTHORS (Last name, first name, middle initial)

Thayaparan, Thayananthan

5. DATE OF PUBLICATION (month and year of publication of document)	6a. NO. OF PAGES (total containing information. Include Annexes, Appendices, etc.)	6b. NO. OF REFS (total cited in document)
September 2004	69	38

7. DESCRIPTIVE NOTES (the category of the document, e.g. technical report, technical note or memorandum. If appropriate, enter the type of report, e.g. interim, progress, summary, annual or final. Give the inclusive dates when a specific reporting period is covered.)

DRDC Ottawa Technical Memorandum

8. SPONSORING ACTIVITY (the name of the department project office or laboratory sponsoring the research and development. Include the address.)

Defence R&D Canada – Ottawa
Ottawa, Ontario, Canada K1A 0Z4

9a. PROJECT OR GRANT NO. (if appropriate, the applicable research and development project or grant number under which the document was written. Please specify whether project or grant)	9b. CONTRACT NO. (if appropriate, the applicable number under which the document was written)
12pz01	

10a. ORIGINATOR'S DOCUMENT NUMBER (the official document number by which the document is identified by the originating activity. This number must be unique to this document.)	10b. OTHER DOCUMENT NOS. (Any other numbers which may be assigned this document either by the originator or by the sponsor)
DRDC Ottawa TM 2004-170	

11. DOCUMENT AVAILABILITY (any limitations on further dissemination of the document, other than those imposed by security classification)

(X) Unlimited distribution
( ) Distribution limited to defence departments and defence contractors; further distribution only as approved
( ) Distribution limited to defence departments and Canadian defence contractors; further distribution only as approved
( ) Distribution limited to government departments and agencies; further distribution only as approved
( ) Distribution limited to defence departments; further distribution only as approved
( ) Other (please specify):

12. DOCUMENT ANNOUNCEMENT (any limitation to the bibliographic announcement of this document. This will normally correspond to the Document Availability (11). However, where further distribution (beyond the audience specified in 11) is possible, a wider announcement audience may be selected.)

13. ABSTRACT (a brief and factual summary of the document. It may also appear elsewhere in the body of the document itself. It is highly desirable that the abstract of classified documents be unclassified. Each paragraph of the abstract shall begin with an indication of the security classification of the information in the paragraph (unless the document itself is unclassified) represented as (S), (C), or (U). It is not necessary to include here abstracts in both official languages unless the text is bilingual).

(U) Mechanical vibrations or rotations (micro-motion dynamics) of structures on a target may introduce frequency modulation on the radar return from the target's body. The modulation due to this vibration or rotation is called the micro-Doppler (m-D) phenomenon. In this report, the m-D effect is introduced and the mathematics of micro-Doppler signatures, induced by the simple sinusoidal vibrations or rotations, is developed. Simulated results confirm that the mathematical analysis is valid. The m-D features derived from a target's vibrational/rotational motion are extracted by utilizing discrete wavelet transforms. During this process, the time domain radar signal is decomposed into a set of components that are represented by different wavelet scales. The m-D features are extracted by sorting the components that are associated with the vibrational/rotational motions of a target and is achieved by applying the inverse wavelet transform. After the extraction of m-D features, time-frequency analysis is employed to analyse the oscillation and to estimate the motion parameters. The vibration/rotation rate is estimated by taking the autocorrelation of the time sequence data. The results show that these results have higher precision after the m-D extraction since only vibrational/rotational components are employed. The proposed method of the m-D extraction has been successfully applied to simulated data. The preliminary results clearly demonstrate that the m-D signatures can be observed by radar and suggest that applications of m-D should be investigated and exploited, and for target detection, classification and recognition. It is recommended that the exploitation of micro-Doppler, as a new identification/recognition tool, be undertaken as it could impact all aspects of radar sensing and may enhance the effectiveness of Automatic Target Recognition (ATR) and Automatic Gait Recognition (AGR) techniques. We recomment that a new man-portable ``micro-Doppler radar" be constructed for use on the battlefield or disaster scenarios. We also propose a sequence of research work to achieve the desired technical objectives.

14. KEYWORDS, DESCRIPTORS or IDENTIFIERS (technically meaningful terms or short phrases that characterize a document and could be helpful in cataloguing the document. They should be selected so that no security classification is required. Identifiers such as equipment model designation, trade name, military project code name, geographic location may also be included. If possible keywords should be selected from a published thesaurus. e.g. Thesaurus of Engineering and Scientific Terms (TEST) and that thesaurus-identified. If it is not possible to select indexing terms which are Unclassified, the classification of each should be indicated as with the title.)

Micro-Doppler
Feature Extraction
Detection
Classification
Recognition
Microwave radar
Automatic Target Recognition
Automatic Gait Recognition
Human Gait
Time-Frequency Distribution
High Range Resolution
Fourier Transform
Doppler Smearing
wavelet